

Review

## Large Scale Cosmological Anomalies and Inhomogeneous Dark Energy

Leandros Perivolaropoulos

Department of Physics, University of Ioannina, Ioannina 45110, Greece; E-Mail: leandros@uoi.gr; Tel.: +30-265-100-8632; Fax: +30-265-100-8698

Received: 6 November 2013; in revised form: 24 December 2013 / Accepted: 25 December 2013 / Published: 17 January 2014

---

**Abstract:** A wide range of large scale observations hint towards possible modifications on the standard cosmological model which is based on a homogeneous and isotropic universe with a small cosmological constant and matter. These observations, also known as “cosmic anomalies” include unexpected Cosmic Microwave Background perturbations on large angular scales, large dipolar peculiar velocity flows of galaxies (“bulk flows”), the measurement of inhomogeneous values of the fine structure constant on cosmological scales (“alpha dipole”) and other effects. The presence of the observational anomalies could either be a large statistical fluctuation in the context of  $\Lambda$ CDM or it could indicate a non-trivial departure from the cosmological principle on Hubble scales. Such a departure is very much constrained by cosmological observations for matter. For dark energy however there are no significant observational constraints for Hubble scale inhomogeneities. In this brief review I discuss some of the theoretical models that can naturally lead to inhomogeneous dark energy, their observational constraints and their potential to explain the large scale cosmic anomalies.

**Keywords:** dark energy; cosmological principle; inhomogeneous anisotropic universe

---

### 1. Introduction

The standard cosmological model ( $\Lambda$ CDM) has been established through a wide range of cosmological observations [1] which challenged its validity during the past two decades. The model is based on the following assumptions: cosmological principle (isotropy, homogeneity, general relativity, cold dark matter and baryonic matter), flatness of space, the existence of a cosmological constant and gaussian scale invariant matter perturbations generated during inflation. Based on these assumptions, the

model makes well defined predictions which are consistent with the vast majority of cosmological data. Some of these predictions include the following:

- **The Cosmic Microwave Background (CMB) Spectrum:** The angular power spectrum of CMB primordial perturbations [2] is in good agreement with the predictions of  $\Lambda$ CDM. However, a few issues related to the orientation and magnitude of low multipole moments (CMB anomalies) constitute remaining puzzles for the standard model [3–11].
- **The statistics of CMB perturbations:** These statistics [12] are consistent with the prediction of gaussianity of the standard model [13].
- **Accelerating expansion:** Cosmological observations using standard candles [Type Ia Supernovae (SnIa)] [14] and standard rulers (Baryon Acoustic Oscillations) [15] to map the recent accelerating expansion rate of the universe are consistent with the existence of a cosmological constant. No need has appeared for more complicated models based on dynamical dark energy or modified gravity, despite of the continuously improved data. The likelihood of the cosmological constant *vs.* more complicated homogeneous models has been continuously increasing during the past decade [16].
- **Large Scale Structure:** Observations of large scale structure are in good agreement with  $\Lambda$ CDM [17] (basic statistics of galaxies [18], halo power spectrum [19]).

Despite of the above major successes the standard model is challenged by a few puzzling large scale cosmological observations [20,21] which may hint towards required modifications of the model. Some of these challenges of  $\Lambda$ CDM may be summarized as follows:

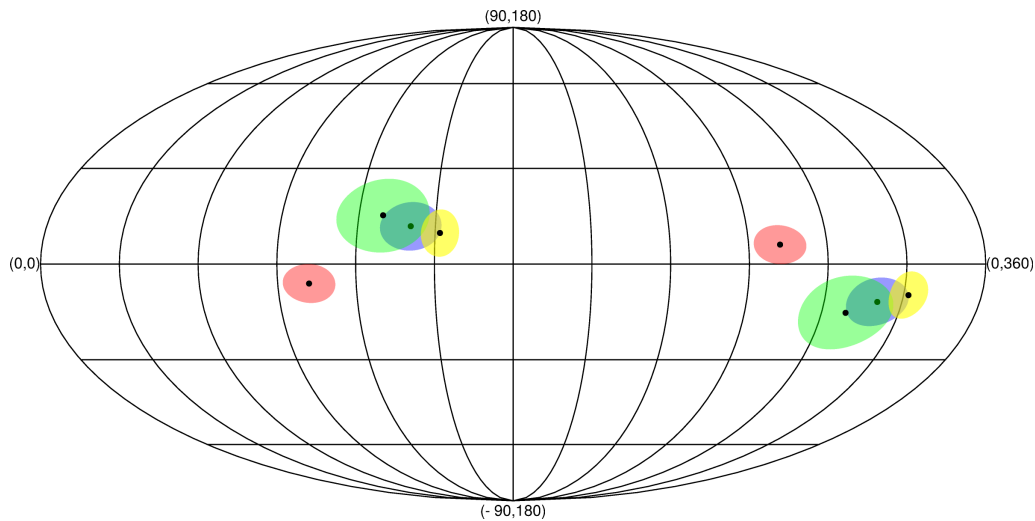
1. **Power Asymmetry of CMB perturbation maps:** A hemispherical power asymmetry in the cosmic microwave background (CMB) on various different angular scales (multipole ranges) has been detected [22–25]. The power in all multipole ranges is consistently found to be significantly higher in the approximate direction towards Galactic longitude and latitude ( $l = 237^\circ, b = -20^\circ$ ) than in the opposite direction. A more recent study of the WMAP9 data has found a hemispherical directional dependence of  $\Lambda$ CDM cosmological parameters which is maximized at the direction ( $l = 227^\circ, b = -27^\circ$ ) at the multipole range 2–600 and is statistically significant at the  $3.4\sigma$  level [26]. A related asymmetry, is the Maximum Temperature Asymmetry (MTA) defined as the maximized temperature difference between opposite pixels in the sky which shows significant alignment with other apparently unrelated asymmetries [27].
2. **Large Scale Velocity Flows:** Recent studies have indicated the existence of dipole velocity flows on scales of  $100 h^{-1}$  Mpc [28,29] with magnitude about 400 km/s using a combination of peculiar velocity surveys, with direction towards  $l \simeq 282^\circ, b \simeq 6^\circ$ . Other studies [30] using the kinematic S-Z effect have found bulk flows on much larger scales ( $O(1$  Gpc)) with magnitude 600–1000 km/s towards a similar direction. These results are inconsistent with the predictions of  $\Lambda$ CDM at a level of 99%. These studies however have been challenged by other authors which do not confirm these results but find peculiar velocities on these scales consistent with  $\Lambda$ CDM [31]. Even though these studies agree with the direction of the observed flow they disagree on the magnitude and errorbar of the measured velocities.

3. **Alignment of low multipoles in the CMB angular power spectrum:** The normals to the octopole and quadrupole planes are aligned with the direction of the cosmological dipole at a level inconsistent with Gaussian random, statistically isotropic skies at 99.7% [4]. This inconsistency has been reduced by the recent Planck results to a level of about 98% [22] (the exact level varies slightly depending on the foreground filtering method).
4. **Large scale alignment in the QSO optical polarization data:** Quasar polarization vectors are not randomly oriented over the sky with a probability often in excess of 99.9%. The alignment effect seems to be prominent along a particular axis in the direction  $(l, b) = (267^\circ, 69^\circ)$  [32–34].
5. **Anisotropy in Accelerating Expansion Rate:** Recent studies of the accelerating cosmic expansion rate using SNIa as standard candles have indicated that an anisotropic expansion rate fit by a dipole provides a better fit to the data than an isotropic expansion rate at the  $2\sigma$  level [35]. Interestingly, this dark energy dipole is abnormally aligned [35] with the fine structure constant dipole discussed below.
6. **Spatial dependence of the value of the fine structure constant  $\alpha$ :** A spatial cosmic variation of the fine structure constant has been recently identified on redshifts up to  $z \simeq 4.2$  by analyzing the absorption spectra of quasars. This anisotropy analysis of the fine structure constant  $\alpha$  [36,37] is based on a large sample of quasar absorption-line spectra (295 spectra) obtained using UVES (the Ultraviolet and Visual Echelle Spectrograph) on the VLT (Very Large Telescope) in Chile and also previous observations at the Keck Observatory in Hawaii. An apparent variation of  $\alpha$  across the sky was found. It was shown to be well fit by an angular dipole model  $(\frac{\Delta\alpha}{\alpha}) = A \cos \theta + B$  where  $\theta$  is the angle with respect to a preferred axis and  $A, B$  are the dipole magnitude and an isotropic monopole term. The dipole axis was found to point in the direction  $(l, b) = (331^\circ, -14^\circ)$  and the dipole amplitude  $A$  was found to be  $A = (0.97 \pm 0.21) \times 10^{-5}$ . The statistical significance over an isotropic model was found to be at the  $4.1\sigma$  level.
7. **Large Quasar Group:** An elongated structure of quasars with long dimension about 1240 Mpc and mean redshift  $\bar{z} = 1.27$  has recently been discovered [38]. This structure is a factor of about three larger than the previously known largest structure (Sloan Great Wall ( $\bar{z} = 0.073$  and comoving size 450 Mpc [39]) and appears to be inconsistent with the cosmological principle in the context of the standard  $\Lambda$ CDM model in the sense that it is much larger than the scale of homogeneity in the context of  $\Lambda$ CDM (260–370 Mpc [40]).

The above seven large scale puzzles are large scale effects (1 Gpc or larger) and seem to be related to violation of the cosmological principle. In fact preferred cosmological directions may be associated with most of them. As discussed in more detail in Section 3, some of these directions appear to be abnormally close to each other. These directions are shown in Figure 1 [27]. This may be an indication for a common physical origin at least for some of the above anomalies.

These anomalies may be simply large statistical fluctuations that manifest themselves due to a posteriori selection of particular statistical tests. In view of their diverse nature and their high statistical significance, is not likely that they are all of this nature. In view of the possibility that there is a physical mechanism that leads to their existence, it is of interest to identify classes of physical models that could predict the existence of some or all of the above cosmic anomalies.

**Figure 1.** Directions in galactic coordinates for the  $\alpha$  (blue) and Dark Energy (green) dipoles, for the Dark Flow direction (red) and for the direction of Maximum Temperature Asymmetry (MTA) in the 7 years ILC CMB map degraded to  $N_{side} = 8$  (yellow). The opposite corresponding directions are also shown (from [27]).



The origin of the possible violation of the cosmological principle could be either geometric or energetic. A geometric origin would correspond to inherent properties of the cosmic metric (e.g., non-trivial topology on large scales). An energetic origin would correspond to non-trivial properties of the energy momentum tensor of the contents of the universe (e.g., anisotropic dark energy equation of state).

Models based on geometric violation of the cosmological principle include the following:

- A multiply connected non-trivial cosmic topology [41,42].
- A rotating universe coupled to an anisotropic scalar field [43].
- Non-commutative geometry [44].
- A fundamental anisotropic curvature [45].

Models based on energetic violation of the cosmological principle include:

- Anisotropic dark energy equation of state [46–48] due perhaps to the existence of vector fields [49,50].
- Dark matter perturbations on a few Gpc scale [51,52]. For example an off center observer in a 1 Gpc void would experience the existence of a preferred cosmological axis through the Lemaître-Tolman-Bondi metric [53–57]. Within this framework, an additional dark energy component is not needed to secure consistency with the cosmological data that indicate accelerating expansion. The basic idea is that the increased expansion rate occurs locally in space rather than at recent cosmological times, a fact that can be achieved by assuming a locally-reduced matter energy density [58,59]. Thus, the observer is placed close to the center of a giant void with dimensions of a few Gpc [60]. Even though this approach is free of dark energy, it is by no means free of fine tuning. Apart from the unnatural assumption of giant-size Gpc voids, which are very unlikely to be produced in any cosmology, these models require the observer to be placed within a very small volume at the center of the void (about  $10^{-6}$  of the total volume of the void). A

slightly off-center observer, however, will naturally experience a preferred cosmological direction (towards the center of the void), which may help to resolve some of the observational puzzles of  $\Lambda$ CDM discussed above.

Such matter perturbations could be induced by statistically anisotropic or non-gaussian primordial perturbations [61–64]. For example, inflationary perturbations induced by vector fields [65–68]. Note however that inflationary models with vector fields usually suffer from instabilities due to the existence of ghosts [69–71].

- Large scale electromagnetic fields [72]. For example, the existence of a large scale primordial magnetic field [73–75]. Evidence for such a magnetic field has recently been found in CMB maps [76].
- Dark energy perturbations on scales comparable to the horizon. Even though the sound speed for dark energy is close to unity implying that it can not cluster on scales much smaller than the horizon, it can still produce observable effects due to clustering on horizon scales [77,78]. In addition the possible recent formation of topological defects with Hubble scale core (topological quintessence) could also behave as inhomogeneous dark energy [79].

Models based on matter underdensities (voids) on scales larger than 1 Gpc are severely constrained by observations [54,80–83] and do not reduce to  $\Lambda$ CDM for any value of their parameters. For radii as large as the horizon they reduce to homogeneous open CDM matter dominated universe and for small radii they reduce to flat CDM models without a cosmological constant. Both of these classes are ruled out by observations. Even for radii of order a few Gpc these models are faced by severe problems that can be summarized as follows:

- There is no simple physical mechanism to generate such large voids [84].
- As discussed above, off center observers experience a CMB dipole that is in excess of the observed one. Thus our location is constrained to practically coincide with the center of the void (fine tuning) to within about a fraction of a percent in radius [85,86].
- The fit for the expansion rate as a function of redshift is worse than  $\Lambda$ CDM requires significant fine tuning of the void profile to obtain a comparable fit with  $\Lambda$ CDM [86].
- These models predict significant peculiar velocities for distant galaxies within the void. Such velocities could have been detected in CMB maps through the kinematic S-Z effects. The fact that such large radial velocities are not observed imposes the most severe class of constraints in this class of models [82].

In contrast to matter void models, spherically inhomogeneous dark energy models are more natural and reduce to  $\Lambda$ CDM when the inhomogeneity radius exceeds the horizon scale. They constitute one of the two generic generalizations of  $\Lambda$ CDM. Instead of breaking time translation invariance of the cosmological constant (as is the case for quintessence models) inhomogeneous dark energy models break space translation invariance of  $\Lambda$ . This corresponds to addressing the coincidence problem of  $\Lambda$ CDM not as “why now?” question but as a “why here?” question. The motivation for considering this class of inhomogeneous dark energy models may be summarized as follows:

- It is a new generic generalization of  $\Lambda$ CDM including  $\Lambda$ CDM as a special case.

- It naturally violates the cosmological principle on large cosmic scales and predicts a preferred axis for off center observers. Thus it has the potential to address at least some of the above discussed cosmic anomalies.
- There is a well defined physical mechanism that can give rise to this type of dark energy inhomogeneities. This mechanism will be discussed in some detail in Section 3. It is based on applying the principles of *topological inflation* [87] to the case of late-time acceleration. According to the idea of topological inflation, the false vacuum energy of the core of a topological defect can give rise to accelerating expansion if the core size reaches the Hubble scale when gravity starts dominating the dynamics. Thus, for example, a recently formed global monopole with appropriate scale of symmetry breaking and coupling could naturally produce a Hubble-scale, spherically symmetric, isocurvature dark energy overdensity. By analogy with topological inflation, this mechanism may be called *topological quintessence*.

In this review we focus on models which can violate the cosmological principle via energy momentum tensor effects (energetic origin violations). Since Hubble scale matter inhomogeneities are severely constrained we consider mainly dark energy Hubble scale inhomogeneities and/or anisotropies which appear to be a more natural source of a mild violation of the cosmological principle.

The structure of this review is the following: In the next section we present a collective analysis of the above discussed cosmic anomalies. After describing in some detail the current observational status of each one of these anomalies we discuss the statistical significance of its incompatibility with large scale homogeneity and isotropy. In Section 3 we describe theoretical models that predict the existence of anisotropic or inhomogeneous dark energy and the potential of these models to explain some of the cosmic anomalies. We discuss two classes of models: Anisotropic dark energy models described by a Bianchi I cosmic metric with anisotropic dark energy equation of state and spherical inhomogeneous dark energy models described by a generalization of the Lemaître-Tolman-Bondi metric. A special case of the later class of models is “topological quintessence” where a well defined physical mechanism generates the spherical dark energy inhomogeneity. Finally in Section 4 we conclude and summarize our results. We also present an outlook discussing remaining open questions and possible future directions of research related to this subject.

## 2. A Review of Cosmic Anomalies

In this section we discuss in some detail the cosmological observations that hint towards a possible violation of the large scale homogeneity and isotropy of the universe.

### 2.1. Power Asymmetry of CMB Perturbation Maps

As discussed in the Introduction, the power spectrum of CMB fluctuations as measured by Wilkinson Microwave Anisotropy Probe (WMAP) and Planck is not isotropic. A hemispherical asymmetry has been pointed out in several studies [2,22,26,71,88–90] using both the WMAP [2] and the Planck data [22] at several multipole ranges. The persistence of this asymmetry in different multipole ranges along with the good multifrequency component separation (especially in the Planck data) make

it unlikely that the asymmetry is due to foregrounds. The observed asymmetry is modeled as a power spectrum dipolar modulation of an otherwise statistically isotropic sky:

$$\Delta T(\hat{n}) = (1 + A\hat{p} \cdot \hat{n})\Delta T_{iso}(\hat{n}) \quad (1)$$

where  $\hat{p}$  and  $\hat{n}$  are unit vectors towards the dipole and the sky directions respectively and  $\Delta T_{iso}(\hat{n})$  is a statistically isotropic temperature fluctuation in the direction  $\hat{n}$ . The best fit dipole is found to have direction  $(l, b) = (227, -27)$  and amplitude  $A = 0.072 \pm 0.022$  for the multipole range  $l < 64$  ( $k < 0.035 \text{ Mpc}^{-1}$ ) [22]. The derived amplitude is inconsistent with isotropy ( $A = 0$ ) at the  $3.4\sigma$  level. If this dipole modulation of the angular power spectrum is not a statistical fluctuation and has a physical cause, then this cause should be such as to change the amplitude of *density* fluctuations by less than  $O(10^{-3})$  as constrained by the CMB dipole magnitude. This is not easy to achieve for a primordial mechanism since the same mechanism responsible for an  $O(10^{-1})$  (as seen by the value of  $A$ ) modulation of the primordial density perturbation spectrum should practically leave unaffected the magnitude of these density perturbations. This however would be easier to achieve for a late time mechanism operating after the density perturbations have been created.

On smaller scales ( $k \sim 1 \text{ Mpc}^{-1}$ ) there is lack of asymmetry in primordial density perturbations as constrained by the SDSS quasar sample [91]. The power spectrum of these quasars is found to be isotropic with  $A < 0.0153$  (at  $3\sigma$ ) for a dipole oriented in the direction of the CMB power asymmetry dipole.

Thus, the possible mechanism that leads to the observed CMB power asymmetry at the  $O(10^{-1})$  level should affect the magnitude of the density perturbations at a level less than  $10^{-3}$  and should also not create power asymmetry on scales  $k \sim 1 \text{ Mpc}^{-1}$  at a level more than about  $O(10^{-2})$ .

Both of these constraints of this physical mechanism are consistent with a late generation of asymmetry through through large scale dark energy inhomogeneities which affect locally the growth of structures and thus the CMB maps through the ISW effect. On the other hand, it is hard to construct primordial models of inflation that satisfy the above two constraints [92,93].

It has been shown recently [94] that a large part of the asymmetry is due to the ISW effect. In the context of inhomogeneous dark energy, regions of denser dark energy would be associated more pronounced ISW effect. Thus there are two hints that point out to the possible late time origin of the CMB asymmetry:

- A large part (if not all) of the asymmetry appears to be due to the ISW effect which occurs at late times and is not related to the primordial nature of the CMB perturbations [94].
- The power spectrum of large scale structure does not show evidence for such a dipole asymmetry on smaller scales. This also hints towards a possible late time origin of the asymmetry.

Dark energy inhomogeneities is clearly a prime candidate that could lead to the generation of late time asymmetry without affecting the spectrum of density perturbations.

## 2.2. Alignment of Low Multipoles in the CMB Angular Power Spectrum

The alignment of the normals to the octopole and quadrupole planes has been verified by several studies [3,6,7,95–98]. The majority of these studies conclude that this is not a foreground contamination

of the WMAP Internal Linear Combination (ILC) maps but rather is an effect degraded by the foregrounds [99,100] (see however [101] for an alternative point of view). The directions of the quadrupole and the octopole are determined by rotating the coordinate system while determining the multipole coefficients  $a_{lm}$ . The coordinate system that maximized the sum  $|a_{ll}|^2 + |a_{l-l}|^2$  is selected and the direction of its  $z$ -axis defines the direction of the  $l$  multipole moment ( $l = 2$  for the quadrupole and  $l = 3$  for the octopole). This coordinate system maximizes the power of fluctuations at its  $x - y$  plane (equator). The exact direction of these moments varies slightly in accordance with the method used to filter the foregrounds.

According to the recent Planck data [22] and one of the filtering methods used, the octopole plane normal is in the direction  $(l, b) = (246^\circ, 66^\circ)$ , and the quadrupole plane normal is in the direction  $(l, b) = (228^\circ, 60^\circ)$ . For comparison the CMB dipole moment is in the direction  $(l, b) = (264^\circ, 48^\circ)$  [102].

The angle between the quadrupole and the octopole directions is found to be in the range  $9^\circ$ – $13^\circ$  depending on the foreground cleaning method used [22]. The probability that this occurs by chance in a random simulation of the best-fit  $\Lambda$ CDM model is found to be about 2%. The alignment however gets significantly degraded by subtracting any large scale specific feature (hot or cold spot) on the CMB map. Thus, it appears there is no specific CMB feature responsible for the alignment. Instead, the alignment appears to be an unlikely statistical fluctuation of amplitudes and phases which could be justified by the a posteriori selection of the particular statistic [5]. Despite the degraded statistical significance of this anomaly by the Planck data it remains an unlikely feature in the context of  $\Lambda$ CDM hinting towards statistical anisotropy. A well defined theoretical model that could naturally justify its existence would have to naturally produce a combination of large scale features in a single CMB map plane leading to the observed alignment.

### 2.3. Large Scale Velocity Flows

The kinematic Sunyaev-Zeldovich (kSZ) effect is a spectral distortion on the CMB photons induced by the coherent velocities of the free electrons in cluster due to the peculiar velocity of the cluster as a whole. A bulk flow of clusters would produce spectral distortions at the locations of clusters whose anisotropy would be well described by a dipole. This method was first applied for the measurement of large scale bulk flows of clusters in [103]. It has the advantage that it is independent of other conventional methods to measure peculiar velocities which require the measurement of distances. In addition it can easily probe scales up to the horizon which is currently impossible with conventional methods. In general however it is not easy to distinguish the small signal of the kSZ dipole from the much larger signal of the intrinsic CMB dipole. Despite of these difficulties the authors of [30,104,105] used a sample of 700 X-Ray selected clusters with redshifts up to  $z \sim 0.2$  (scale of about 800 Mpc) and detected a persistent kSZ dipole which they interpreted as evidence for bulk flow of clusters with magnitude 600–1000 km/s in a direction  $l \simeq 296^\circ \pm 28^\circ$ ,  $b \simeq 39^\circ \pm 14^\circ$ .

Other studies however have not confirmed this result [106–110] using somewhat different methodologies and datasets. Most of these studies [106,108,110] have obtained a similar dipole but have claimed significantly larger errors which make the derived magnitudes of bulk flows statistically



insignificant and consistent with null (and with  $\Lambda$ CDM which predicts much smaller coherent peculiar velocities on these scales). The issue remains controversial [111] and there is currently a debate as to the identification of the proper methodology for the implementation of the kSZ effect to derive the peculiar velocities of clusters.

On smaller scales (50–100  $h^{-1}$ Mpc), an application of a Minimal Variance weighting algorithm to a compilation of 4481 peculiar velocity measurements [28] lead to a bulk flow of  $407 \pm 81$  km/s towards  $l \simeq 287^\circ \pm 9^\circ$ ,  $b \simeq 8^\circ \pm 6^\circ$ . This result is inconsistent (too large) with respect to  $\Lambda$ CDM normalized on WMAP7 at a level of 98% while the direction of the flow is consistent with the result of [104]. A more recent analysis [112] using the peculiar velocities of a sample of 245 SnIa has obtained a bulk flow of a lower magnitude ( $248 \pm 87$  km/s) towards a similar direction  $l \simeq 319^\circ \pm 25^\circ$ ,  $b \simeq 7^\circ \pm 13^\circ$ . This magnitude of the bulk flow is marginally consistent with both  $\Lambda$ CDM and with the previous analysis of [28] and its direction is even closer to other anisotropy directions discussed below (dark energy dipole,  $\alpha$  dipole and CMB cold spot I [27]). Consistent results with  $\Lambda$ CDM are also obtained by [113] using SnIa peculiar velocities to measure bulk flows.

#### 2.4. Large Scale Alignment in the QSO Optical Polarization Data

The optical polarization properties of 355 quasars with redshifts up to  $z \sim 2.5$  and with well defined polarization angles were studied in [33] (see also [32]). The cosmic scales covered are up to about 2 Gpc. It was found that the quasar polarization vectors are not randomly distributed in the sky at a confidence level of 99.9%. Sources of systematics like instrumental and interstellar polarizations were carefully considered and shown not to affect the main conclusions of the analysis. In addition, the polarizations of quasars obtained by different observatories were found to agree within the uncertainties in both polarization degree and angle. The observed large scale angular correlations of quasar polarization in regions sized at least 1 Gpc showed a coherent change of the mean polarization angle with redshift. The effect appeared stronger along an axis close to the CMB dipole even though direction uncertainties are large. If the effect is not due to an unknown systematic or due to a large statistical fluctuation, it may be evidence for departure from the cosmological principle (large scale isotropy).

An interesting physical mechanism [34] that could lead to the observed coherent rotation of quasar polarizations with redshift involves a coupling between the photon and a pseudoscalar (e.g., axion) in a Lagrangian of the form:

$$\mathcal{L} = \frac{1}{2}(\partial_\mu\phi)(\partial^\mu\phi) - \frac{1}{2}m^2\phi^2 - \frac{1}{4}F_{\mu\nu}F^{\mu\nu} - j_\mu A^\mu + \frac{1}{4}g\phi F_{\mu\nu}\tilde{F}^{\mu\nu} \quad (2)$$

where  $\tilde{F}^{\mu\nu}$  is the dual Maxwell tensor and  $\frac{1}{4}g\phi F_{\mu\nu}\tilde{F}^{\mu\nu}$  describes the mixing pseudoscalar axions and photons. In the context of such a Lagrangian, photons with polarization parallel to a weak external magnetic field decay into pseudoscalars leading to a net polarization  $p$ . Thus coherent variation of the polarization  $p$  over cosmological distances are predicted provided that there is a magnetic field  $B < 1$  nG [114].

If there is a variation of the direction of  $\vec{B}$  with distance then a rotation of the polarization angle with redshift is predicted. In an extended model where the pseudovector  $\phi$  also plays the role of quintessence with induced inhomogeneities a correlation between accelerating expansion and quasar polarization would be anticipated.

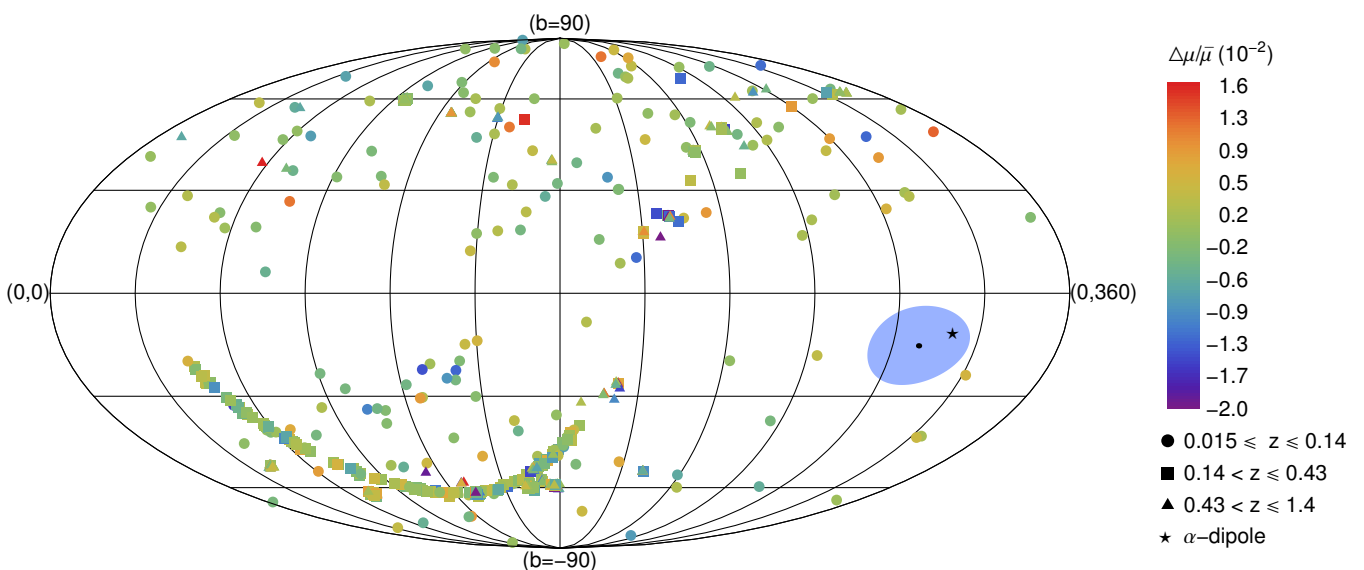
Recent data showing a similar polarization alignment of radiowaves [115] on scales up to 1 Gpc however appear to impose constraints on the pseudoscalar coupling mechanism [116]. Similar strong constraints on this mechanism are imposed by the observed lack of circular polarization in the quasar data [117].

### 2.5. Anisotropy in Accelerating Expansion Rate (Dark Energy Dipole)

Several recent studies [35,118–129] have investigated the isotropy of the accelerating cosmological expansion rate at various redshift ranges using samples of SnIa as standard candles. Most studies search for a preferred direction using either a hemisphere comparison method [118,120,121,123,129] or a fit to a dipole angular distribution of the anisotropy [35,122,125,128] (dark energy dipole). There are indications [35] that the dipole fit may be more sensitive in identifying the expansion anisotropy signal than the hemisphere comparison method. The consensus of these studies is that there is an asymmetry axis pointing in the direction ( $l \simeq 310^\circ, b = -15^\circ$ ) which is roughly consistent with the direction of the CMB Cold Spot I [5]. This asymmetry is more prominent for low redshift SnIa ( $z \leq 0.2$ ) perhaps due to the fact that there are significantly more and better quality SnIa data for this redshift range [35]. The magnitude of the asymmetry is marginally consistent with  $\Lambda$ CDM (at about  $2\sigma$  level). The direction of this asymmetry axis appears to be consistent at  $1\sigma$  with both the peculiar velocity flows direction and with the alpha dipole direction discussed below (Figure 2).

The approximate coincidence of these four preferred directions (dark flow, dark energy dipole,  $\alpha$  dipole and CMB cold spot) may hint towards a possible common physical origin for these anomalies.

**Figure 2.** The distribution of the Union2 SnIa datapoints in galactic coordinates along with the Dark Energy dipole direction are shown. The datapoints are split in three different redshift bins shown with different shapes. The direction of the  $\alpha$ -dipole is also shown with a star. The light blue blob represents the  $1-\sigma$  error on the Dark Energy dipole direction (from [35]).



## 2.6. Anisotropy in the Values of the Fine Structure Constant $\alpha$ ( $\alpha$ Dipole)

The absorption spectra of distant quasars contain two pieces of information: the redshift of the absorber and the value of the fine structure constant  $\alpha$ . This information extracted by the Many Multiplet Method has been used to perform an anisotropy analysis of the fine structure constant  $\alpha$  [36,37]. The analysis is based on a large sample of quasar absorption-line spectra (295 spectra) obtained using UVES (the Ultraviolet and Visual Echelle Spectrograph) on the VLT (Very Large Telescope) in Chile and also previous observations at the Keck Observatory in Hawaii.

An apparent variation of  $\alpha$  across the sky was found. It was shown to be well fit by an angular dipole model  $\left(\frac{\Delta\alpha}{\alpha}\right) = A \cos\theta + B$  where  $\theta$  is the angle with respect to a preferred axis and  $A, B$  are the dipole magnitude and an isotropic monopole term. The dipole axis was found to point in the direction  $(l, b) = (331^\circ, -14^\circ)$  and the dipole amplitude  $A$  was found to be  $A = (0.97 \pm 0.21) \times 10^{-5}$ . The statistical significance over an isotropic model is at the  $4.1\sigma$  level. The analysis of [36,37] has received criticism [130–132] based mainly on the fact that its quasar sample combines two datasets (Keck and VLT) with different systematic errors which have a small overlapping subset and cover opposite hemispheres on the sky. The axis connecting these two hemispheres has similar direction with the direction of the obtained dipole. The response of the authors of [36,37] was based on the fact that in the equatorial region of the dipole, where both the Keck and VLT samples contribute a number of absorbers, there is no evidence for inconsistency between Keck and VLT.

The angular separation between the Dark Energy Dipole direction and the  $\alpha$  dipole is found to be only  $11.3^\circ \pm 11.8^\circ$ . Reference [35] used Monte Carlo simulations to find the probability of obtaining the observed dipole magnitudes with the observed alignment, in the context of an isotropic cosmological model with no correlation between dark energy and fine structure constant  $\alpha$ . It was found that this probability is less than one part in  $10^6$ .

A simple physical model (extended topological quintessence [35,79]) naturally predicts a spherical inhomogeneous distribution for both dark energy density and fine structure constant values. The model is based on the existence of a recently formed giant global monopole with Hubble scale core which also couples non-minimally to electromagnetism. Aligned dipole anisotropies would naturally emerge for an off-centre observer for both the fine structure constant and for dark energy density. This model smoothly reduces to  $\Lambda$ CDM for proper limits of its parameters. Two predictions of this model are (a) a correlation between the existence of strong cosmic electromagnetic fields and the value of  $\alpha$  and (b) the existence of a dark flow on Hubble scales due to the repulsive gravity of the global defect core (“Great Repulser”) aligned with the dark energy and  $\alpha$  dipoles. The direction of the dark flow is predicted to be towards the spatial region of lower accelerating expansion. Existing data about the dark flow [28,30] are consistent with this prediction. In the next section we present a detailed analysis of this model.

## 2.7. Large Quasar Groups

According to SDSS DR7 for galaxies with  $0.22 < z < 0.50$  [133], isotropy appears to be established on scales larger than 210 Mpc as anticipated from the overall isotropy of the CMB. However, on larger redshifts, isotropy appears to be challenged by recent quasar data.

The Large Quasar Groups (LQG) are large structures of quasars appearing at redshifts  $z \approx 1$  with scales 70–350 Mpc. A new elongated LQG was discovered recently [38] in the DR7QSO catalogue of the Sloan Digital Sky Survey [134]. It has long dimension 1240 Mpc and characteristic size  $(Volume)^{1/3}$  about 500 Mpc at a redshift  $z = 1.27$  (Huge-LQG). It is located in the direction  $l = 225^\circ$ ,  $b = 63^\circ$ , relatively close (distance of boundaries 140 Mpc) to another fairly large LQG and consists of 73 member quasars. The principal axes of the LQG have lengths of 1240, 640, and 370 Mpc extending to the Gpc-scale. According to [40], the upper limit to the scale of homogeneity for the concordance cosmology is 370 Mpc. Their long dimensions from the inertia tensor of 630 and 780 Mpc are clearly much larger than the anticipated upper limit of homogeneity. It is the currently known largest structure in the universe and maybe at odds with the cosmological principle [40]. We stress however that other more recent studies have indicated [135,136] that such structures may not be inconsistent with a homogeneous Poisson distribution of quasars. Indeed, such structures seem to be discovered [135,136] by the algorithm of [38] in explicitly homogeneous simulations of a Poisson point process with the same density as the quasar catalogue.

### 3. Anisotropic/Inhomogeneous Dark Energy Models

In view of the successes of the standard  $\Lambda$ CDM model it is anticipated that a viable theoretical model able to explain the above described anomalies should have the following properties:

- Deviate from  $\Lambda$ CDM mainly on large cosmological scales.
- Reduce to  $\Lambda$ CDM for certain values of its parameters.

In addition, it appears reasonable and in fact hinted by some of the above described data that the physical origin of the deviation from isotropy resides at late cosmological times when these large scales are again causally connected (consider, e.g., the possible ISW origin of the CMB power asymmetry [94]). Motivated by these arguments and by the discussion presented in the Introduction we focus on models involving anisotropic and/or inhomogeneous dark energy. In contrast to matter, dark energy can be anisotropic (due to its pressure) without being inhomogeneous and also the possible inhomogeneities of dark energy naturally appear on Hubble scales where the origin of the anomalies seems to reside. In addition, Gpc inhomogeneities (voids) of matter constitute models that do not smoothly reduce to  $\Lambda$ CDM for any value of their parameters. This class of models has been shown to be severely constrained by several cosmological observations and especially the kSZ effect which is predicted to be significantly larger in these models than observations indicate [82]. Thus in what follows we focus on models of anisotropic/inhomogeneous dark energy.

#### 3.1. Anisotropic Dark Energy Models

A generic generalization of the Friedmann-Lemaître-Robertson-Walker (FLRW) metric that introduces anisotropy but not inhomogeneity is the Bianchi I metric which is of the form:

$$ds^2 = -dt^2 + a^2(t)dx^2 + b^2(t)dy^2 + c^2(t)dz^2 \quad (3)$$

Such a metric is consistent with an energy momentum tensor of a fluid with homogeneous but anisotropic pressure of the form:

$$T_{\nu}^{\mu} = \text{diag}(-1, w_x, w_y, w_z)\rho \quad (4)$$

where  $(w_x, w_y, w_z)$  are the equation of state componenets corresponding to each component of pressure. The deviation of these components may be parametrised by two parameters [137]  $\gamma$  and  $\delta$ . Using these parameters, the anisotropic dark energy energy momentum tensor Equation (4) may be expressed as:

$$T_{\nu}^{\mu} = \text{diag}(-1, w, w + 3\delta, w + 3\gamma)\rho \quad (5)$$

The deviations from isotropy may be quantified by defining the average Hubble expansion rate  $H$  and the Hubble normalized shear  $R$  and  $S$  as:

$$H \equiv \frac{1}{3} \left( \frac{\dot{a}}{a} + \frac{\dot{b}}{b} + \frac{\dot{c}}{c} \right) \quad (6)$$

and

$$R \equiv \frac{1}{H} \left( \frac{\dot{a}}{a} - \frac{\dot{b}}{b} \right), \quad S \equiv \frac{1}{H} \left( \frac{\dot{a}}{a} - \frac{\dot{c}}{c} \right) \quad (7)$$

The generalized Friedmann equation is then obtained as:

$$H^2 = \frac{8\pi G}{3} \frac{\rho + \rho_m}{1 - \frac{1}{9}(R^2 + S^2 - RS)} \quad (8)$$

where  $\rho_m$  is the matter density which in general is allowed to interact with dark energy. Conservation of the energy momentum tensor of anisotropic dark energy implies:

$$\dot{\rho} + 3 \left[ (1 + w) H + \delta \frac{\dot{b}}{b} + \gamma \frac{\dot{c}}{c} \right] \rho = -QH\rho_m \quad (9)$$

where  $\rho_m$  is the matter density which obeys:

$$\dot{\rho}_m + 3H\rho_m = QH\rho \quad (10)$$

and a nonzero value of the parameter  $Q$  expresses the interaction between dark energy and matter. Such an anisotropic dark energy could emerge for example in the presence of a vector field  $A_{\mu}$  whose dynamics is described by the action [137]:

$$S = \int d^4x \sqrt{-g} \left[ \frac{R}{16\pi G} - \frac{1}{4} F_{\mu\nu} F^{\mu\nu} - V \right] \quad (11)$$

where  $F_{\mu\nu} = \partial_{\mu}A_{\nu} - \partial_{\nu}A_{\mu}$  and the potential  $V$  is a function of  $A^2 = A_{\mu}A^{\mu}$  [137].

The main observational effect of anisotropic dark energy is its contribution to the CMB anisotropies at the level of low multipole moments. This contribution is introduced through the last scattering redshift which becomes anisotropic in the context of the metric Equation (3). For a photon observed from the a direction  $\hat{\mathbf{p}}$  the last scattering redshift  $z$  may be obtained using the lightlike geodesic equatios. It is of the form:

$$1 + z(\hat{\mathbf{p}}) = \frac{1}{a} \sqrt{1 + \hat{p}_y^2 e_y^2 + \hat{p}_z^2 e_z^2} \quad (12)$$

where:

$$e_y^2 = \left(\frac{a}{b}\right)^2 - 1, \quad e_z^2 = \left(\frac{a}{c}\right)^2 - 1 \quad (13)$$

are evaluated at the time of last scattering and the scale factors are all normalized to unity today. Thus, the predicted CMB temperature is of the form:

$$T(\hat{\mathbf{p}}) = T_*/(1 + z(\hat{\mathbf{p}})) \quad (14)$$

where  $T_*$  is the temperature at decoupling. Using the spatial average  $4\pi\bar{T} = \int d\Omega_{\hat{\mathbf{p}}} T(\hat{\mathbf{p}})$ , the temperature anisotropies is expressed as:

$$\frac{\delta T(\hat{\mathbf{p}})}{\hat{T}} = 1 - \frac{T(\hat{\mathbf{p}})}{\bar{T}} \quad (15)$$

This anisotropy may be expanded in spherical harmonics to evaluate the contribution to all CMB multipole moments and thus impose constraints on the parameters  $\gamma$  and  $\delta$  by demanding that these multipoles do not exceed the observed values. Significant fine tuning is required on the anisotropy parameters to secure consistency with the observed low quadrupole value [137–139].

Less stringent constraints on the anisotropy parameters may be obtained by considering the isotropy of the accelerating cosmic expansion rate as determined using the luminosity distances of SNIa. The predicted values of luminosity distances in the context of the metric Equation (3) is obtained [137] at the redshift  $z$  in the direction  $\hat{\mathbf{p}}$  as:

$$d_L(z, \hat{\mathbf{p}}) = (1 + z) \int_{t_0}^{t(z)} \frac{dt}{\sqrt{\hat{p}_x^2 a^2 + \hat{p}_y^2 b^2 + \hat{p}_z^2 c^2}} \quad (16)$$

where  $z$  is connected with the scale factors via Equation (12). Using the maximum likelihood method and the observed luminosity distances it is possible to obtain constraints on the anisotropy parameters  $\gamma$  and  $\delta$  and show that their absolute values are constrained to be less than about 0.1 at the  $3\sigma$  level [137].

An alternative parametrization of the dark energy anisotropy involves the consideration the anisotropic stress  $\sigma$ . This is obtained by expressing the dark energy momentum tensor as [138]:

$$T_{\mu\nu} = \rho u_\mu u_\nu + p(g_{\mu\nu} + u_\mu u_\nu) + \Sigma_{\mu\nu} \quad (17)$$

where where  $u_\mu$  is the four-velocity of the fluid, and  $\Sigma_{\mu\nu}$  is the anisotropic stress tensor. The anisotropic stress  $\sigma$  is defined as:

$$(\rho + p)\sigma = -(\hat{k}_i \hat{k}_j - \frac{1}{3}\delta_{ij})\Sigma_{ij} \quad (18)$$

The anisotropic stress  $\sigma$  quantifies the deviation of pressure from isotropy. As discussed in [137], only weak constraints can be imposed on  $\sigma$  using recent data.

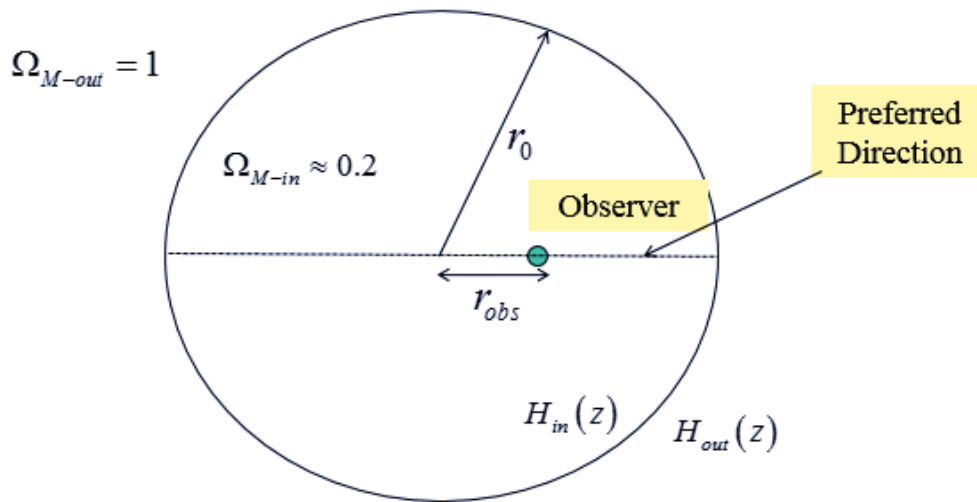
The introduction of anisotropic dark energy as described above provides the potential for breaking of statistical isotropy and resolution of some of the large scale anomalies discussed in the previous section. In particular, the anisotropic pressure can induce peculiar velocity flows, anisotropy in the SNIa data and significant CMB dipole and quadrupole [137]. The most severe constraints on the level of anisotropy originate from the CMB observed isotropy but these can be softened by considering a time dependent anisotropy which is more significant at late times and consistent with the weaker constraints originating from the SNIa data.

### 3.2. Inhomogeneous Dark Energy Models

In the context of inhomogeneous cosmologies, the simplest way to introduce a preferred direction in the universe is to consider a Hubble scale spherical dark matter void or dark energy inhomogeneity and an off center observer. In the case of dark matter void, an observer close to the center of the void will detect a larger Hubble parameter for nearby points in space and lower redshift. Thus she may incorrectly interpret it as an accelerating expansion rate since the Hubble expansion will appear higher at lower redshifts. Thus a spatial variation of expansion rate may be misinterpreted as a temporal variation. In the case of a spherical dark energy overdensity the variation of the expansion rate is both spatial and temporal and there is a true accelerating expansion rate amplified by the spatial variation of the dark energy density.

The displacement direction will be naturally preferred and the observer will experience anisotropic accelerated Hubble expansion and Hubble scale velocity flows (Figure 3). In fact the center of the dark matter void or dark energy overdensity will behave as a great repulser inducing velocity flows away from it.

**Figure 3.** An off-center observer in a spherical inhomogeneity sees a preferred direction of higher accelerating expansion rate.



As a simple toy model we may consider an inhomogeneous fluid of matter and/or dark energy described by the energy-momentum tensor:

$$T_{\nu}^{\mu} = \text{diag}(-\rho(r) - \rho_M(r, t), p_r(r), p_t(r), p_t(r)) \quad (19)$$

The general spherically symmetric inhomogeneous cosmological spacetime is described by the metric [140–142]:

$$ds^2 = -dt^2 + A^2(r, t)dr^2 + B^2(r, t) (d\theta^2 + \sin^2 \theta d\varphi^2) \quad (20)$$

In the special case of a diagonal energy momentum tensor as the one of Equation (19), the above metric takes the simplified form [140–142]:

$$ds^2 = -dt^2 + \frac{(B'(r, t))^2}{1 - k(r)} dr^2 + B^2(r, t) (d\theta^2 + \sin^2 \theta d\varphi^2) \quad (21)$$

where  $B(r, t)$  is the spacetime dependent scale factor and  $k(r)$  plays the role of inhomogeneous spherically symmetric spatial curvature. In the limit of a homogeneous spacetime, the LTB metric Equation (21) reduces to the FLRW metric by setting  $k(r)$  to a constant and  $B(r, t) = ra(t)$ . Using the metric Equation (21) and the energy momentum tensor Equation (19) in the Einstein equations we obtain the generalized Friedman equation:

$$H^2(r, t) = H_0^2(r) \left[ \Omega_M(r) \left( \frac{B_0}{B} \right)^3 + \Omega_X(r) + \Omega_c(r) \left( \frac{B_0}{B} \right)^2 \right] \quad (22)$$

where:

$$H(r, t) \equiv \frac{\dot{B}(r, t)}{B(r, t)} \quad (23)$$

with  $B_0(r) \equiv B(r, t_0)$  ( $t_0$  is the present time),  $H_0(r) \equiv H(r, t_0)$ ,  $\Omega_X(r) \equiv -8\pi G p_r(r)/3H_0^2(r)$  (which is positive for negative radial pressure) and  $\Omega_c(r) \equiv 1 - \Omega_X(r) - \Omega_M(r)$ . The profile of the inhomogeneous dark energy pressure,  $\Omega_X(r)$ , is in principle arbitrary, and is physically determined by the physical mechanism that induced the inhomogeneous overdensity.

Interesting density profiles of the inhomogeneities (dark matter and dark energy) which parametrize the inside and outside densities ( $\Omega_{in}$  and  $\Omega_{out}$ ) as well as the interface thickness ( $\Delta r$ ) are of the form:

$$\Omega_M(r) = \Omega_{M,out} + (\Omega_{M,in} - \Omega_{M,out}) \frac{1 - \tanh[(r - r_0)/2\Delta r]}{1 + \tanh(r_0/2\Delta r)} \quad (24)$$

$$\Omega_X(r) = \Omega_{X,out} + (\Omega_{X,in} - \Omega_{X,out}) \frac{1 - \tanh[(r - r_0)/2\Delta r]}{1 + \tanh(r_0/2\Delta r)} \quad (25)$$

It is straightforward to solve Equation (22) by first determining  $H_0(r)$  in units of  $\text{Gyr}^{-1}$ , assuming an age of the universe  $t_0 = 13.7$  Gyr (homogeneous Big Bang). We thus use:

$$H_0(r) = \frac{1}{t_0} \int_0^1 \frac{dx}{\sqrt{\Omega_M(r)x^{-1} + \Omega_X(r)x^2 + \Omega_c(r)}} \quad (26)$$

which can be easily derived from Equation (22). With Equation (26) equation and the initial condition  $B(r, t_0) = r$  we solve Equation (22) and obtain numerically  $B(r, t)$  and its derivatives.

For an observer in the center of the spherical inhomogeneity, light travels radially inwards and therefore for these lightlike geodesics  $d\theta = d\phi = 0$  along the geodesic. The remaining two light-like geodesics for radially *incoming* light rays are of the form [143]:

$$\frac{dt}{dz} = - \frac{B'(r, t)}{(1+z)\dot{B}(r, t)} \quad (27)$$

$$\frac{dr}{dz} = \frac{c\sqrt{1-k(r)}}{(1+z)\dot{B}(r, t)} \quad (28)$$

where  $c \simeq 0.3$  is the velocity on light in units of Gpc/Gyr used for consistency in order to obtain the luminosity distance in Gpc. Using these lightlike geodesics with initial conditions  $t(z=0) = t_0$  and  $r(z=0) = 0$  we find  $t(z)$  and  $r(z)$ . The angular diameter and luminosity distances are then obtained as:

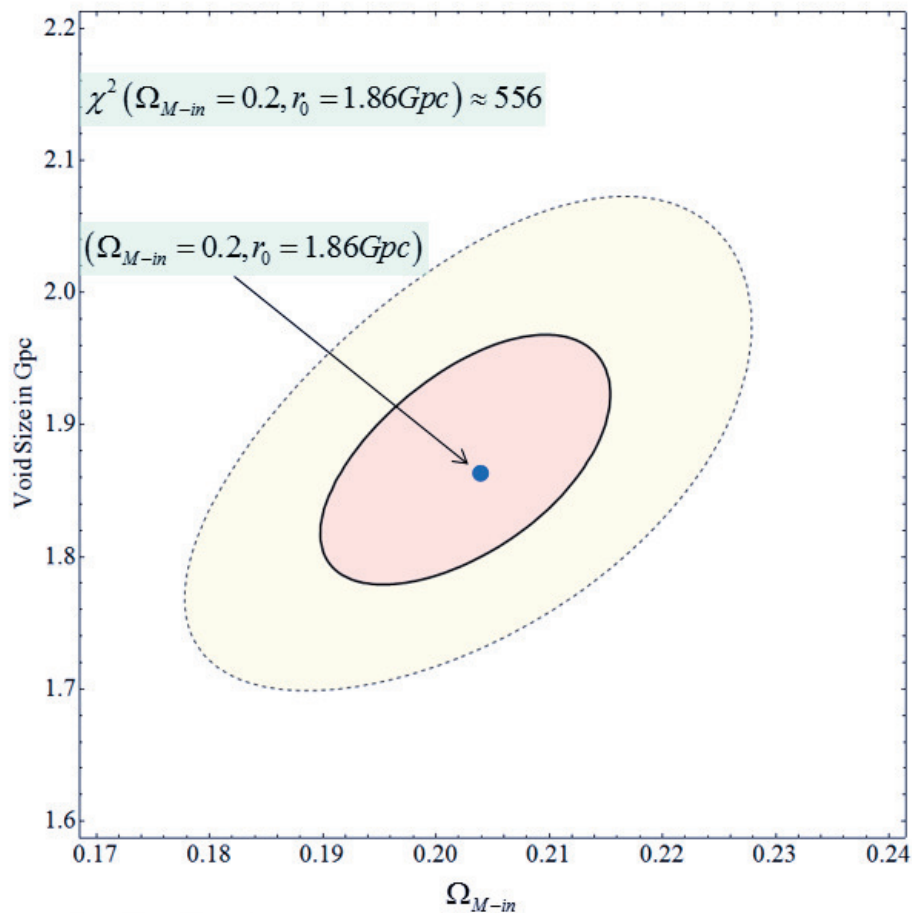
$$d_A(z, r_0, \Omega_{X,in}) = B(r(z), t(z)) \quad (29)$$

$$d_L(z, r_0, \Omega_{X,in}) = (1+z)^2 d_A(z) \quad (30)$$



Using the above form of the luminosity distance, it is straightforward to fit the predicted distance moduli to the observed ones from the Union2 dataset and derive the best-fit values of parameters for the on-center observer. We first consider a dark matter inhomogeneity (void) with no dark energy. Fixing the interface thickness to  $\Delta r = 0.35$  Mpc,  $\Omega_{X,in} = \Omega_{X,out} = 0$  (no dark energy),  $\Omega_{M,out} = 1$ , it is straightforward to obtain [86] the  $1\sigma$  and  $2\sigma$  contours for the parameters  $\Omega_{M,in}$  (matter underdensity inside the void) and  $r_0$  (size of the void) shown in Figure 4.

**Figure 4.** The  $1\sigma$  and  $2\sigma$  contours for the parameters  $\Omega_{M,in}$  (matter underdensity inside the void) and  $r_0$  (size of the void) (from [86]).



This class of Gpc void models had until recently attracted significant attention. They have three main advantages:

- They are consistent with the observed redshift dependence of the Hubble expansion rate as obtained using standard candles SnIa [143,144] without the requirement of dark energy.
- They can naturally provide a preferred axis by utilizing a slight displacement of the observer from the center of the spherical void.
- The coincidence problem is not present since a void can naturally develop at late times along with other structures.

Despite of the above successes, it has been evident that this class of models also suffers from significant problems. As discussed in the Introduction, these problems include the following:

- In the context of standard cosmology there is no simple mechanism to create Gpc matter voids without conflicting other cosmological data (e.g., CMB fluctuations).
- If the observer location is not fine tuned close to the center of the spherical void, then a CMB dipole is predicted which is larger than the observed [85,86].
- There is no simple matter density profile that will provide an equal or better quality of fit compared to  $\Lambda$ CDM [86].
- This class of models generically predicts large peculiar velocities of free electrons and clusters with respect to the CMB. These velocities could have been detected via inverse Compton scattering of CMB photons onto moving free electrons (kinematic Synyaev-Zeldovich effect). The existing bounds on such velocities effectively rules out this class of models [82,83].

In view of the above problems of matter void models (see also [54]), it is of some interest to consider models where the Gpc void is replaced by a dark energy spherical overdensity with similar size. As discussed in the Introduction, the motivation for this class of inhomogeneous dark energy models may be summarized as follows:

- The standard cosmological model  $\Lambda$ CDM assumes the existence of homogeneous matter on large scales, the validity of general relativity and the existence of homogeneous dark energy with constant in time energy density (cosmological constant). The generalization of most of these assumptions has been extensively studied in the literature. The main motivation for such generalizations originates at the coincidence problem expressed as a “Why now?” problem: “Why was the energy scale of the cosmological constant tuned to such low values so that it starts dominating at the present time?”. For example general relativity has been generalized to various models of modified gravity, dark energy was allowed to evolve in time as a scalar field (quintessence), matter was allowed to be inhomogeneous on Gpc scales (void models). The least studied generalization is the one based on allowing dark energy to become inhomogeneous on Gpc scales. Such a generalization could in principle address the coincidence problem if the later is expressed as a “Why here?” problem: “Why is the dark energy density in our horizon such that the universe has recently started its accelerating expansion?”. In the same manner that the answer to the “Why now?” question could be time dependence, the answer to the “Why here?” question could be spatial dependence of dark energy density. Therefore, the consideration of inhomogeneous dark energy constitutes a generic generalization of the standard  $\Lambda$ CDM models which reduces back to  $\Lambda$ CDM for a inhomogeneity scale that exceeds the current horizon scale. It is therefore interesting to use cosmological observations to impose constraints on the two basic parameters of this class of models: the scale of the inhomogeneity and the magnitude of the dark energy density inhomogeneity.
- As in the case of the dark matter void, an off-center observer in a spherically symmetric dark energy inhomogeneity will naturally experience an anisotropy in the accelerating expansion rate. In the case of inhomogeneous dark energy the scale of the inhomogeneity is allowed to be as large as the horizon scale ( $\Lambda$ CDM limit). For large enough inhomogeneity scale, the observer is allowed to be displaced significantly from the center without experiencing a large CMB dipole. Thus, inhomogeneous dark energy models are less subject to fine tuning with respect to the location of the observer [86].

- Due to negative pressure and speed of sound close to unity, dark energy inhomogeneities are not easy to sustain. However, there is a well defined physical mechanism (topological quintessence [79]) that can lead to sustainable large scale dark energy inhomogeneities, supported by topological considerations. This mechanism can be viewed as a generalization of topological inflation [87] in which early time accelerating expansion (inflation) takes place in the core of a topological defect due to the topologically trapped vacuum energy.

In this brief review I focus on spherically symmetric dark energy inhomogeneities corresponding to global monopoles in the context of topological quintessence. It is straightforward to generalize this assumption by considering other models that are both inhomogeneous and anisotropic. For example the Szekeres quasi-spherical models [145,146], are effectively non-linear FLRW perturbations [147], with metric of the form:

$$ds^2 = -dt^2 + e^{2A} dx^2 + e^{2B} (dy^2 + dz^2) \quad (31)$$

where  $A = A(t, x, y, z)$ ,  $B = B(t, x, y, z)$ . Such models can be matched to a dust FLRW model across a matter-comoving spherical junction surface [148] and may represent different types of topological defects in the context of topological quintessence (strings or walls).

### 3.3. Topological Quintessence

Topological quintessence [79] assumes the recent formation of a global topological defect (e.g., a global monopole) with Hubble scale core and with core vacuum energy density of the same order as the current density of matter. The dynamics of such a global monopole is determined by the action:

$$S = \int d^4x \sqrt{-g} \left[ \frac{m_{Pl}^2}{16\pi} \mathcal{R} - \frac{1}{2} (\partial_\mu \Phi^a)^2 - V(\Phi) + \mathcal{L}_m \right] \quad (32)$$

where  $\mathcal{L}_m$  is the Lagrangian density of matter fields,  $\Phi^a$  ( $a = 1, 2, 3$ ) is an  $O(3)$  symmetric scalar field and:

$$V(\Phi) = \frac{1}{4} \lambda (\Phi^2 - \eta^2)^2, \quad \Phi \equiv \sqrt{\Phi^a \Phi^a} \quad (33)$$

The vacuum energy density in the monopole core and the size of the core are determined by the two parameters of the model  $\eta$  (the vacuum expectation value) and  $\lambda$  (the coupling constant). The global monopole field configuration is described by the hedgehog ansatz:

$$\Phi^a = \Phi(r, t) \hat{r}^a \equiv \Phi(r, t) (\sin \theta \cos \varphi, \sin \theta \sin \varphi, \cos \theta) \quad (34)$$

with boundary conditions:

$$\Phi(0, t) = 0, \quad \Phi(\infty, t) = \eta \quad (35)$$

where a time dependence is allowed, having in mind a cosmological setup of an expanding background.

The general spherically symmetric spacetime around a global monopole may be described by a metric of the form Equation (20). In order to derive the cosmological dynamical equations we need the total energy momentum tensor  $T_{\mu\nu}$ . We assume a cosmological setup at recent cosmological times and therefore  $T_{\mu\nu}$  is dominated by the global monopole vacuum energy and matter, *i.e.*:

$$T_{\mu\nu} = T_{\mu\nu}^{(mon)} + T_{\mu\nu}^{(mat)} \quad (36)$$

The energy momentum tensor of the monopole is given by:

$$T_{\mu\nu}^{(mon)} = \partial_\mu \Phi^a \partial_\nu \Phi^a - g_{\mu\nu} \left[ \frac{1}{2} (\partial_\sigma \Phi^a)^2 + V(\Phi) \right] \quad (37)$$

The negative pressure in the monopole core is expected to lead to accelerating expansion when the core size is of the order of the Hubble scale [149]. The monopole energy density is of the form:

$$\rho^{mon} = T_{00}^{mon} = \left[ \frac{\dot{\Phi}^2}{2} + \frac{\Phi'^2}{2A^2} + \frac{\Phi^2}{B^2 r^2} + \frac{\lambda}{4} (\Phi^2 - \eta^2)^2 \right] \quad (38)$$

and has a local maximum at the monopole core where vacuum energy dominates. The energy-momentum tensor of matter is that of a perfect fluid with zero pressure ( $p = 0$ ):

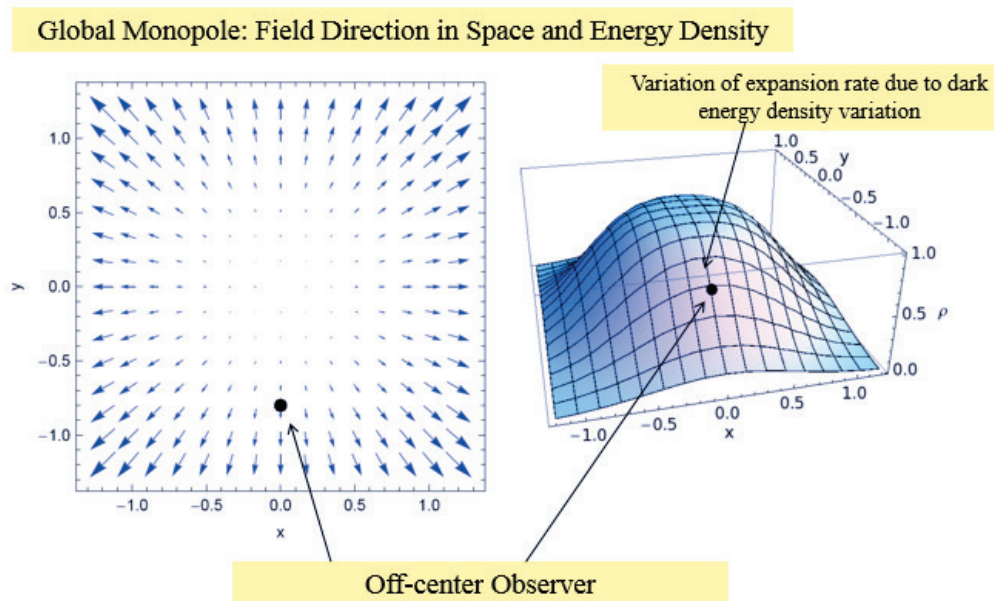
$$T_{\mu\nu}^{(mat)} = \rho^{mat} u_\mu u_\nu \quad (39)$$

where  $\rho^{mat} = \rho^{mat}(r, t)$  is the matter density and  $u^\mu$  is the velocity 4-vector of the fluid:

$$u^\mu = \left( \frac{1}{\sqrt{1-v^2}}, \frac{v}{A\sqrt{1-v^2}}, 0, 0 \right) \quad (40)$$

with  $v = v(r, t)$  the radial matter fluid velocity. An off-center observer in the global monopole will experience anisotropic accelerating cosmological expansion which is maximized in the direction of the monopole center where the vacuum dark energy density is maximum (Figure 5). This is consistent with the mild evidence ( $2\sigma$ ) for the existence of a dark energy dipole discussed in Section 2.

**Figure 5.** An off-center observer in the core of a global monopole will naturally experience an anisotropy in the expansion rate due to the higher vacuum energy density in the direction of the monopole center.



The question that arises is “Can this mechanism also predict the existence of a fine structure constant dipole aligned with the dark energy dipole as seems to be favored by some observations?” The answer to

this question is positive. An  $\alpha$  dipole aligned with the dark energy dipole can be obtained by considering a dilatonic coupling of the monopole scalar field to electromagnetism. Consider the generalization of the Lagrangian Equation (32) of the form:

$$S = \int \left[ \frac{1}{2} M_p^2 R - \frac{1}{2} (\partial_\mu \Phi^a)^2 - V(\Phi) + \frac{1}{4} B(\Phi) F_{\mu\nu}^2 + \mathcal{L}_m \right] \sqrt{-g} d^4x \quad (41)$$

where  $M_p^{-2} = 8\pi G$  is the reduced Planck mass. This action is inspired from the Bekenstein-Sandvik-Barrow-Magueijo class of models [150–152] where the dynamics are attributed to a homogeneous scalar field. In our case (extended topological quintessence) the fine structure constant  $\alpha$  has obtained dynamics through the inhomogeneous global monopole scalar field. It may be shown that:

$$\alpha(\Phi) = \frac{e_0^2}{4\pi B(\Phi)^2} \quad (42)$$

where  $e_0$  is the bare charge that remains constant throughout the cosmological evolution. By considering a dilatonic coupling  $B(\Phi)$  of the form Consider now a non-minimal coupling of the form:

$$B(\Phi) = 1 - \xi \frac{\Phi^2}{\eta^2} \quad (43)$$

where  $\xi$  is constant, we find for small values of  $\Phi/\eta$  a spatial variation of  $\alpha$  in accordance to:

$$\left( \frac{\Delta\alpha}{\alpha} \right) \simeq 2\xi \frac{(\Phi^2 - \Phi_0^2)}{\eta^2} \quad (44)$$

where  $\Phi_0$  is the field magnitude at the location of the observer. Clearly,  $\alpha$  is predicted to vary most in the direction where the field magnitude varies more rapidly. This is the direction towards the center of the monopole which is identical to the direction of the dark energy dipole. Thus, this model naturally predicts the observed alignment between the  $\alpha$  dipole and the dark energy dipole.

The observationally required values of the parameters of topological quintessence may be obtained by implementing the requirement that the core size is comparable to the Hubble scale and the vacuum energy density at the monopole core is comparable to the matter density at present. The core scale (where  $\Phi/\eta \lesssim 1$ ) of the static global monopole is:

$$\delta \simeq \lambda^{-1/2} \eta^{-1} \quad (45)$$

while the vacuum energy density in this core region is:

$$\rho^{core} \simeq \frac{\lambda\eta^4}{4} \quad (46)$$

Deep inside the monopole core the expansion is approximately isotropic ( $A(r, t) \simeq B(r, t) \equiv a_{in}(t)$ ) and the dynamics of the scale factors are approximated by:

$$3H_{in}(t)^2 = \frac{8\pi}{m_{Pl}^2} \left( \frac{\lambda\eta^4}{4} + \rho_{0,in}^{mat} \left( \frac{a_{0,in}}{a_{in}} \right)^3 \right) \quad (47)$$

where  $a_{0,in} \equiv a_{in}(t_0)$  is the scale factor at the present time  $t_0$ ,  $\rho_{0,in}^{mat}$  is the present density of matter in the monopole core and:

$$H_{in}(t) \equiv \left( \frac{\dot{a}_{in}}{a_{in}} \right) \quad (48)$$

Similarly, far away from the monopole core ( $r \gg \delta$ ), spacetime is also approximately homogeneous and we may set  $A(r, t) \simeq B(r, t) \equiv a_{out}(t)$ . In this limit the dynamics of the scale factors are obtained from:

$$3H_{out}(t)^2 = \frac{8\pi}{m_{pl}^2} \rho_{0,out}^{mat} \left( \frac{a_{0,out}}{a_{out}} \right)^3 \quad (49)$$

corresponding to a flat matter dominated universe. By imposing the physical requirements stated above namely:

$$\delta \simeq H_0^{-1} \equiv H_{in}(t_0)^{-1} \quad (50)$$

$$\rho^{core} \simeq \rho^{mat}(t_0) \quad (51)$$

where  $\rho^{core}$  is the vacuum energy density in the monopole core, we obtain order of magnitude estimates for the two parameters in the global monopole action:

$$\eta \sim O(1) \times M_{pl} \quad (52)$$

$$\lambda \sim 10^{-120} \bar{\eta} \quad (53)$$

where  $\bar{\eta} \equiv \frac{\eta}{M_{pl}}$ . In what follows we omit the bar on the dimensionless  $\bar{\eta}$ .

In an effort to go beyond the above heuristic estimates we consider the full Einstein equations and using the metric Equation (20) and the energy-momentum tensor Equation (36) we obtain the system of Equations [79,149,153]:

$$\begin{aligned} -G_0^0 &= K_2^2(2K - 3K_2^2) - 2\frac{B''}{A^2B} - \frac{B'^2}{A^2B^2} + 2\frac{A'B'}{A^3B} - 6\frac{B'}{A^2Br} + 2\frac{A'}{A^3r} - \frac{1}{A^2r^2} + \frac{1}{B^2r^2} \\ &= \frac{8\pi}{m_{pl}^2} \left[ \frac{\dot{\Phi}^2}{2} + \frac{\Phi'^2}{2A^2} + \frac{\Phi^2}{B^2r^2} + \frac{\lambda}{4}(\Phi^2 - \eta^2)^2 + \frac{\rho^{mat}}{1-v^2} \right] \end{aligned} \quad (54)$$

$$\frac{1}{2}G_{01} = K_2^{2'} + \left( \frac{B'}{B} + \frac{1}{r} \right) (3K_2^2 - K) = \frac{4\pi}{m_{pl}^2} \left( \dot{\Phi}\Phi' - \frac{v}{1-v^2} A \rho^{mat} \right) \quad (55)$$

$$\begin{aligned} \frac{1}{2}(G_1^1 + G_2^2 + G_3^3 - G_0^0) &= \dot{K} - (K_1^1)^2 - 2(K_2^2)^2 \\ &= \frac{8\pi}{m_{pl}^2} \left[ \dot{\Phi}^2 - \frac{\lambda}{4}(\Phi^2 - \eta^2)^2 + \frac{1}{2} \frac{1+v^2}{1-v^2} \rho^{mat} \right] \end{aligned} \quad (56)$$

and:

$$\ddot{\Phi} - K \dot{\Phi} - \frac{\Phi''}{A^2} - \left( -\frac{A'}{A} + \frac{2B'}{B} + \frac{2}{r} \right) \frac{\Phi'}{A^2} + \frac{2\Phi}{B^2r^2} + \lambda\Phi(\Phi^2 - \eta^2) = 0 \quad (57)$$

where prime (dot) denotes differentiation with respect to radius  $r$  (time  $t$ ) and:

$$K_1^1 = -\frac{\dot{A}}{A}, K_2^2 = K_3^3 = -\frac{\dot{B}}{B}, K = K_i^i \quad (58)$$

The conservation of the energy momentum tensor for the matter fluid Equation (39) in the metric Equation (20) leads to the following equations for  $v$  and  $\rho^{mat}$ :

$$\frac{\dot{v}}{v} = (v^2 - 1) \frac{\dot{A}}{A} - \frac{v'}{A} \quad (59)$$

$$\frac{\dot{\rho}^{mat}}{\rho^{mat}} = \frac{\dot{v}}{v} - 2\frac{\dot{B}}{B} - \frac{v}{A} \frac{(\rho^{mat})'}{\rho^{mat}} - 2\frac{v}{A} \frac{B'}{B} - \frac{2v}{rA} \quad (60)$$

Notice that in the homogeneous FLRW limit ( $B(r, t) = A(r, t) = a(t)$ ,  $\Phi(r, t) = \eta$ ) we obtain the familiar Friedman equations with  $v = 0$  and the usual conservation of matter equation. The system Equations (54)–(57), (59) and (60) consists of six equations with five unknown functions  $A$ ,  $B$ ,  $\Phi$ ,  $v$ ,  $\rho^{mat}$ . Thus, Equation (54) may be considered as a constraint and the system of the other five equations may be solved with initial conditions corresponding to a homogeneous flat matter dominated universe ( $A = B = 1$ ) with a static global monopole profile  $f(r)$  ( $f(0) = 0$ ,  $f(\infty) = 1$ ) [79]. The main questions to be addresses in such a cosmological simulation are the following:

- Does the monopole energy density eventually dominate over matter in the monopole core?
- Does the possible monopole domination eventually lead to accelerating expansion in the monopole core?
- Can this cosmological expansion in the core fit the cosmological data?

The answer to all three of the above questions turns out to be positive. The evolution of the densities is shown in Figure 6. As expected, matter develops an underdensity in the core due to the repulsive gravity of the vacuum energy.

Clearly the vacuum energy eventually dominates in the monopole core. The time evolution of the scale factors  $A$  and  $B$  is shown in Figure 7 for two values of  $\bar{\eta}$ . Clearly the core experiences a faster (accelerating) expansion compared to regions outside the monopole core. For  $\bar{\eta} > 0.3$  the comoving monopole core size appears to expand in agreement with previous studies of topological inflation.

In Figure 8 we show the evolution of the Hubble expansion rate ratios  $H_A(r, z)/H_A(r, 0)$  and  $H_B(r, z)/H_B(r, 0)$  at various comoving distances from the monopole center. Superposed is shown the  $\Lambda$ CDM Hubble expansion rate for the best fit values of  $\Omega_\Lambda$ . We have chosen the present time such that the best fit value at the core center is  $\Omega_\Lambda = 0.73$ . Clearly the expansion rates at all distances are almost identical with  $\Lambda$ CDM with diminishing choices of  $\Omega_\Lambda$ . Thus, for a core size larger than a few Gpc we anticipate good agreement of the predictions of the model with SNIa and other cosmological data.

**Figure 6.** Evolution of the dark energy (left panel) and properly normalized matter (right panel) density profiles. The profiles shown correspond to the initial time  $t_0$  (dotted line),  $t_p/3$  (dot-dashed line),  $2t_p/3$  (dashed line),  $t_p$  (solid line, present time). Notice the matter underdensity that develops in the monopole core while the monopole density appears to slowly collapse to the center in comoving coordinates. The radial unit is the monopole core size  $\delta$  (from [79]).

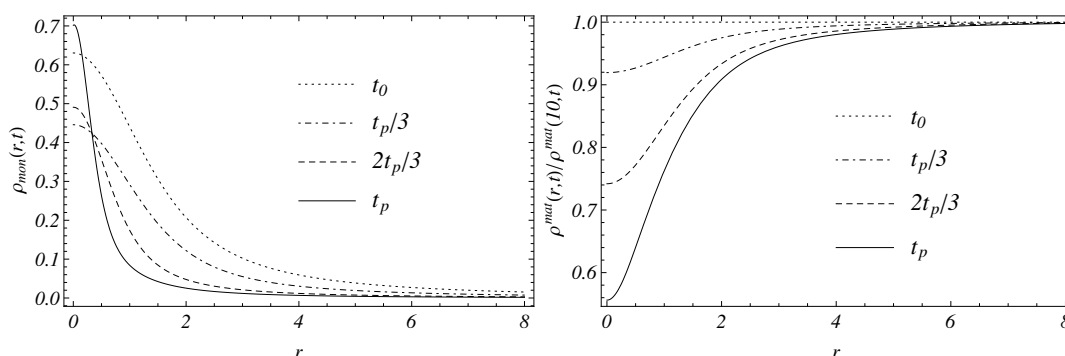


**Figure 7.** Evolution of the scale factors  $A(r, t)$  and  $B(r, t)$  profile for  $\eta = 0.1$  (black lines) and  $\eta = 0.6$  (blue lines) from the time  $t_0$  up to the present time  $t_p$ . A mesh of dots is superimposed to the curve corresponding to  $\eta = 0.1$ ,  $t = t_p$  to distinguish it from the curve obtained for  $\eta = 0.6$ ,  $t = t_p$ . The profiles shown correspond to  $t_0$  (dotted line),  $t_p/3$  (dot-dashed line),  $2t_p/3$  (dashed line),  $t_p$  (solid line). Higher curves correspond to more recent times. The (rescaled) comoving region of accelerated expansion is slightly smaller in the case of  $\eta < 0.3$  since the monopole core does not expand in this case (from [79]).

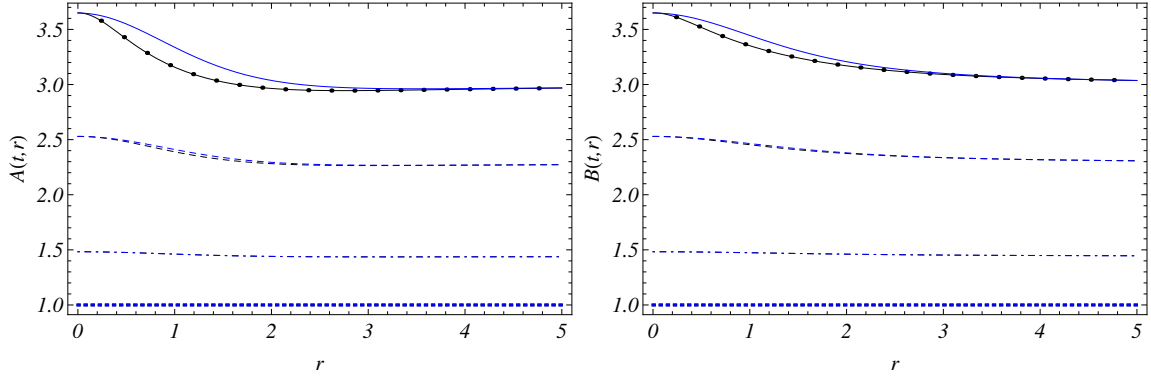
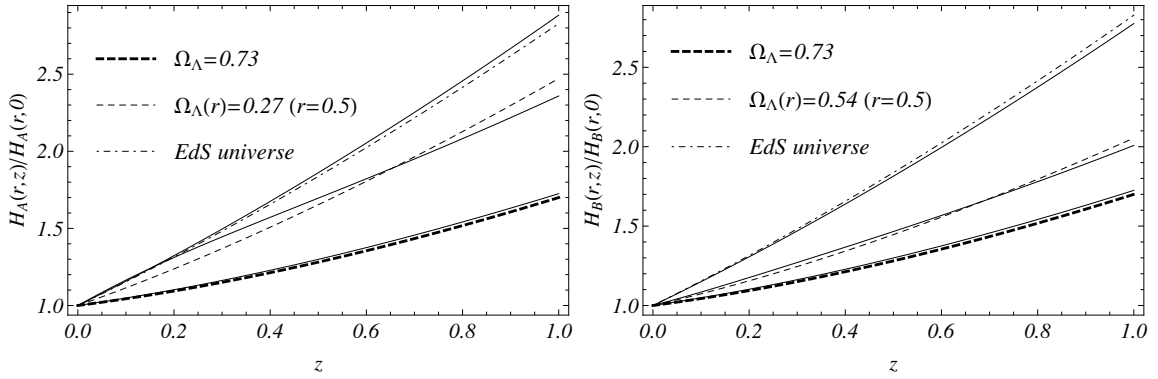


**Figure 8.** Ratios  $H_A(r, z)/H_A(r, 0)$  and  $H_B(r, z)/H_B(r, 0)$  for  $r = 0$  (lower solid line),  $r = 0.5$  and  $r = 5$  (upper solid lines) along with the corresponding  $H_\Lambda(r, z)/H_0$  for  $\Omega_\Lambda = 0.73$  (thick, dashed line) and for  $\Omega_\Lambda = 0$  (dot-dashed line). Also included for comparison  $H_\Lambda(r, z)/H_0$  for the best fit values of  $\Omega_\Lambda(r)$ :  $\Omega_\Lambda(0.5) \simeq 0.27$  (left panel) and  $\Omega_\Lambda(0.5) \simeq 0.54$  (right panel). We have set  $\eta = 0.1$  (from [79]).



### 3.4. Spherical Dark Energy Overdensity

Even though topological quintessence is a well defined physical model based on specific dynamics, the predicted nonlinear evolution of dark energy complicates the detailed comparison with cosmological observation. This comparison, is significantly simplified if we approximate the dark energy inhomogeneity as a static spherically symmetric fluid with negative pressure in a flat background. In particular we may consider the energy momentum tensor:

$$T_\nu^\mu = \text{diag}(-\rho(r) - \rho_M(r, t), p_r(r), p_t(r), p_t(r)) \quad (61)$$



where  $\rho_M(r, t)$  is the matter density and we have allowed for a general inhomogeneous and spherically symmetric static fluid with:

$$(T_f)^\mu_\nu = \text{diag}(-\rho(r), p_r(r), p_t(r), p_t(r)) \quad (62)$$

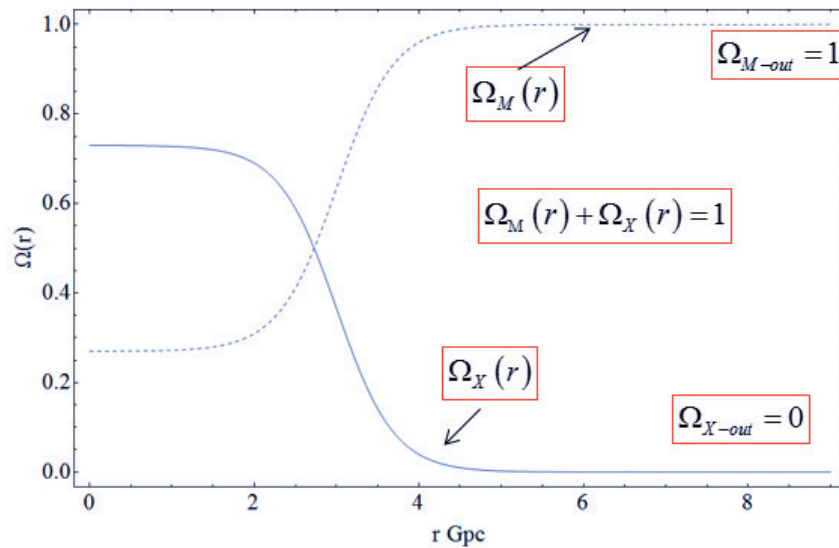
(where  $p_t(r)$  is the transverse pressure). This expression is motivated by the energy-momentum of a global monopole, which asymptotically is of the form [154]:

$$(T_{\text{mon}})^\mu_\nu = \text{diag}(-\eta/r^2, -\eta/r^2, 0, 0) \quad (63)$$

with  $\eta$  the symmetry-breaking scale related to the formation of the monopole.

Using Einstein equations, it may be shown [86] that the metric corresponding to the diagonal energy momentum tensor Equation (61) is of the LTB form Equation (21). Using Einstein equation we obtain the cosmological Equation (22). In contrast to the matter void here we set  $\Omega_c(r) = 0$  and use the profiles Equations (24) and (25) for the matter and dark energy fluids which are consistent with flatness ( $\Omega_{M,\text{out}} = 1 - \Omega_{X,\text{out}} = 1$ , Figure 9).

**Figure 9.** The assumed matter and dark energy profiles are consistent with flatness and with matter domination outside the inhomogeneity. Such profiles would develop dynamically in the context of topological quintessence (see Figure 6).



Considering an observer at the center of the inhomogeneity, we may use the geodesics [86,144] to obtain the luminosity distance as described above Equation (30). By comparing the predicted luminosity distance with the Union 2 data [14], we obtain [86] constraints on the model parameters  $\Omega_{M,\text{in}} = 1 - \Omega_{X,\text{in}}$  and  $r_0$  (the size of the inhomogeneity) using the maximum likelihood method [86]. The allowed range of parameters is significantly larger for the inhomogeneous dark energy model (IDE) and as expected, the model reduces to  $\Lambda$ CDM for a scale of inhomogeneity that is larger than the range of the Union 2 dataset (see Figure 10).

It is straightforward to extend this analysis to the case of an off-center observer [86,155]. In this case the light-like geodesics of the photons coming from the SnIa, depend on two additional parameters: the distance of the observer from the center of the inhomogeneity ( $r_{\text{obs}}$ ) and the incidence angle  $\xi$  of the

photons with respect to the displacement axis (Figure 11). The angle  $\xi$  in turn may be expressed in terms of the direction of the center in galactic coordinates  $(l_c, b_c)$  and the direction the supernova that emits the photon  $(l, b)$  ( $\xi = \xi(l_c, b_c, l, b)$ ). Thus, it is straightforward [86] to obtain an expression of the predicted luminosity distance as  $d_L(z, r_0, \Omega_{X,\text{in}}; r_{\text{obs}}, \xi)$  and use the Union 2 data (with the directions  $(l, b)$  of each SNIa) with the maximum likelihood method to derive  $\chi^2(r_0, \Omega_{X,\text{in}}; r_{\text{obs}}, l_c, b_c)$ .

**Figure 10.** The  $1\sigma$  and  $2\sigma$  parameter contours for the inhomogeneous dark energy (IDE) fluid model obtained using the Union 2 data, compared with the corresponding contours of the usual LTM matter void model. Notice that for an inhomogeneity size larger than the range of the dataset (about 4 Gpc), the model reduces to  $\Lambda$ CDM ( $\Omega_m = 2.7$ ,  $\Omega_X = 0.73$ ). The transition scale was fixed to  $\Delta r = 0.35$  Gpc (from [86]).

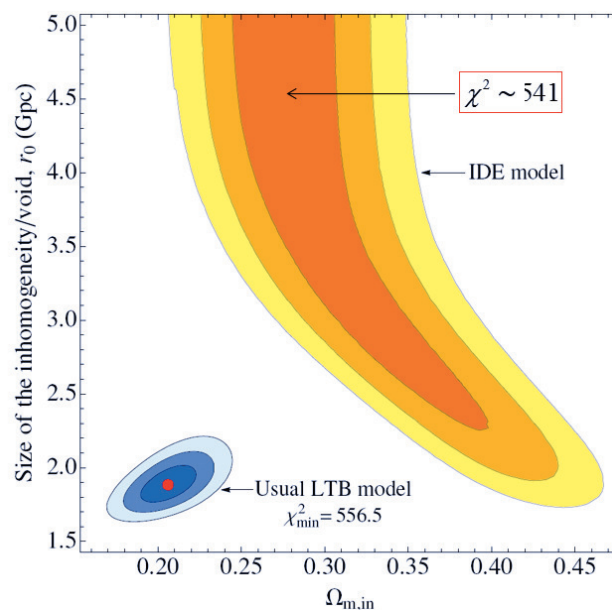
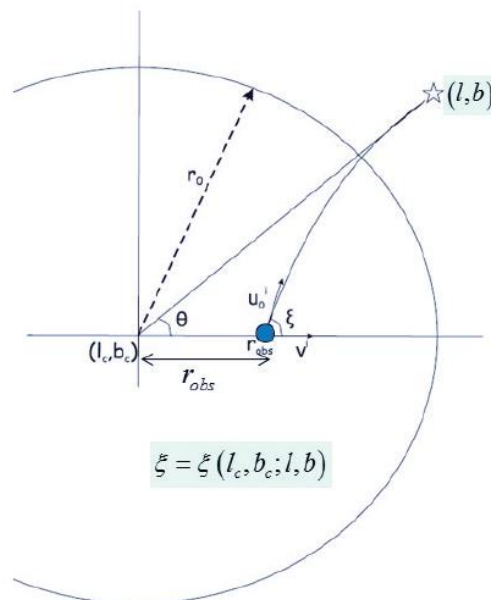
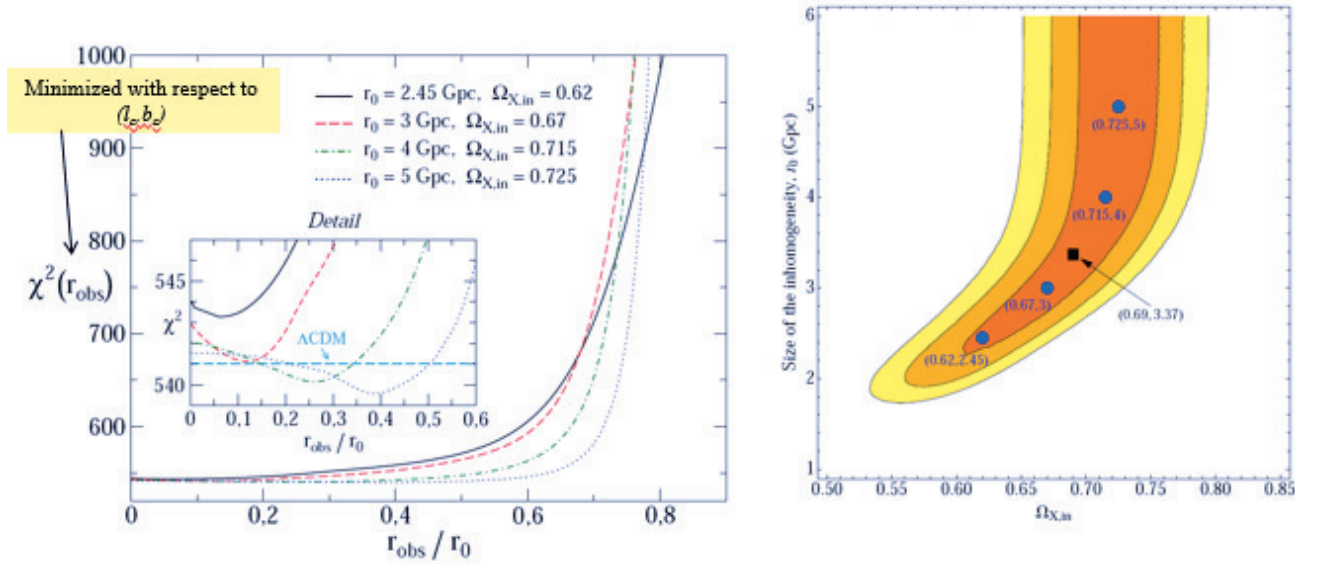


**Figure 11.** The lightlike geodesics for an off-center depend on two additional parameters  $r_{\text{obs}}$  and  $\xi$ .



In Figure 12 we show the dependence of  $\chi^2$  on the displacement  $r_{obs}$  of the observer (left panel). Minimization with respect to the direction of the inhomogeneity center has been performed. We have considered four pairs  $(r_0, \Omega_{X,in})$  that provide good fits for the on center observer (right panel). Notice that improved fit with respect to  $\Lambda$ CDM (horizontal blue dashed line) is obtained only for large scale inhomogeneities ( $r_0 > 3.5$  Gpc).

**Figure 12.** The dependence of  $\chi^2$  on the displacement  $r_{obs}$  of the observer (left panel). Minimization with respect to the direction of the inhomogeneity center has been performed. We have considered four pairs  $(r_0, \Omega_{X,in})$  that provide good fits for the on center observer (right panel). Notice that improved fit with respect to  $\Lambda$ CDM (horizontal blue dashed line) is obtained only for large scale inhomogeneities ( $r_0 > 3.5$  Gpc) (from [86]).



It is straightforward [86] to also use geodesics from the last scattering surface to the present time to derive the CMB photon geodesics for an off center observer. From these we may obtain the last scattering surface redshift  $z_{ls}$  as a function of the inhomogeneity parameters and in particular  $\xi$  and  $r_{obs}$  (assuming fixed the inhomogeneity parameters  $r_0, \Omega_{X,in}$ ). After obtaining  $z_{ls}(\xi, r_{obs})$  we find the angular dependence of the temperature as:

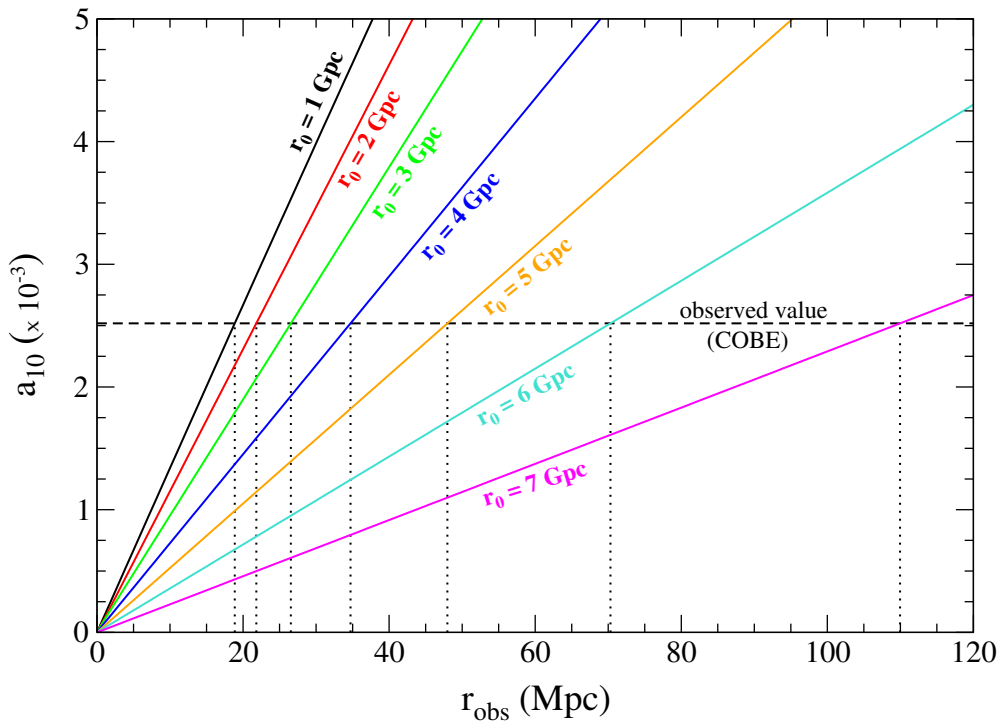
$$T(\xi, r_{obs}) = \frac{T_{ls}}{1 + z_{ls}(\xi, r_{obs})} \quad (64)$$

where  $T_{ls}$  is the observed temperature of the last scattering surface. This is assumed to be uniform since we are focusing on the *additional* temperature fluctuations induced by the displacement of the observer. We then convert it to temperature fluctuations from the mean and expand in spherical harmonics to find the multipole coefficients. Comparison with the measured values of the moments (particularly of the dipole) leads to constraints on  $r_{obs}$ . It is straightforward to obtain numerically  $a_{10}(r_{obs})$ , the additional CMB fluctuations dipole moment induced by the shift  $r_{obs}$  of the observer. This quantity is shown in

Figure 13 for various values of the inhomogeneity scale  $r_0$ . In the same plot we show the value of the measured CMB dipole (dashed line) [156]:

$$\begin{aligned} \left(\frac{\Delta T}{T}\right)_{10} &= \frac{3.35 \times 10^{-3} \text{ K}}{2.725 \text{ K}} = (1.230 \pm 0.013) \times 10^{-3} \\ a_{10} &= \sqrt{\frac{4\pi}{3}} \left(\frac{\Delta T}{T}\right)_{10} \simeq (2.52 \pm 0.03) \times 10^{-3} \end{aligned} \quad (65)$$

**Figure 13.** The predicted CMB dipole moment  $a_{10}(r_{obs})$  for  $\Omega_{X,in} = 0.69$  and various values of the inhomogeneity scale  $r_0$ . The dashed line corresponds to the observed value (whose uncertainty is too small to be shown (from [86])).



Clearly, for  $r_0 < 5$  Gpc the observer is confined to be in a sphere which is a fine tuned small spatial fraction of the dark energy inhomogeneity ( $f(r_0) \equiv (\frac{r_{obs-max}}{r_0})^3 \simeq 10^{-6}$ ) which implies severe fine tuning of the model as in the case of LTB models with matter. This is shown in Figure 14 where  $f(r_0)$  is plotted for values of  $r_0$  between 1 and 7 Gpc. As shown in that figure, the fine tuning starts to reduce ( $f(r_0)$  increases) as the size of the inhomogeneity increases beyond 6 Gpc. We anticipate it to disappear as the size of the inhomogeneity reaches  $\sim 14$  Gpc (the comoving distance to the last scattering surface).

The predicted CMB maps of additional temperature fluctuations in galactic coordinates corresponding to the full map (a), dipole (b) quadrupole (c) and octopole (d) are shown in Figure 15. Notice the rapid decrease of the magnitude of moments higher than the dipole. Even though the order of magnitude of the dipole and quadrupole is comparable with observations, higher moments have negligible magnitude. This is anticipated since the displacement of the observer is expected to modify the CMB fluctuations only at the largest scales.

**Figure 14.** The spatial fraction  $f(r_0) \equiv \left(\frac{r_{obs-max}}{r_0}\right)^3$  where the observer needs to be confined in order to be consistent with the value of the observed CMB dipole, for  $(r_0, \Omega_{X,in}) = (3.37 \text{ Gpc}, 0.69)$  (from [86]).

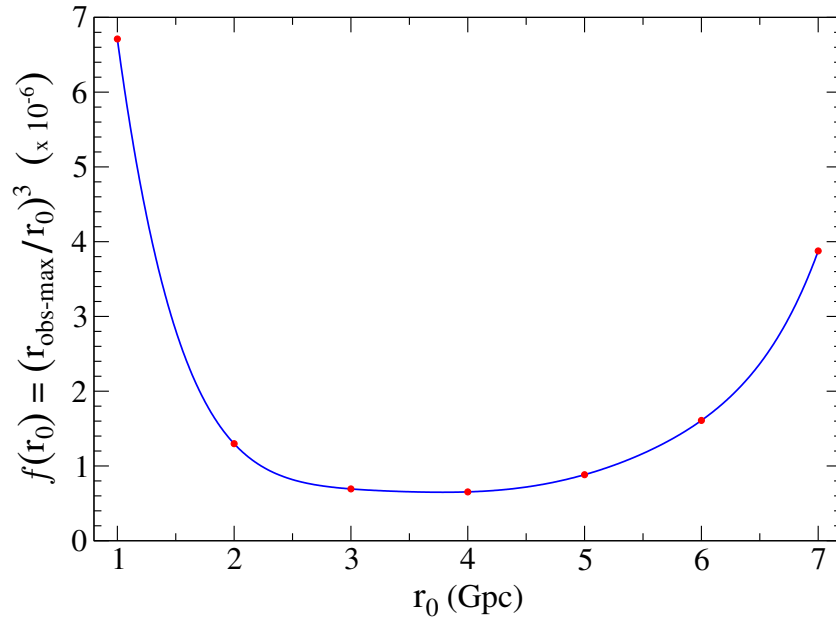
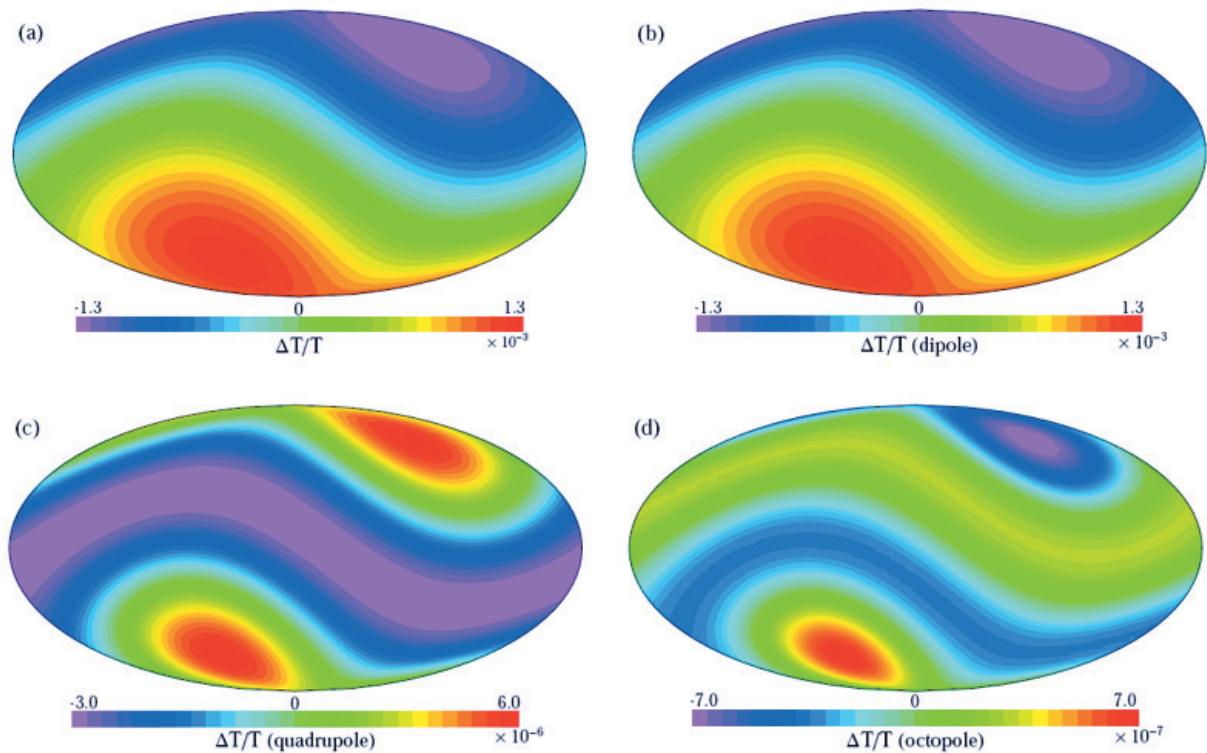


**Figure 15.** The predicted CMB maps of additional temperature fluctuations in galactic coordinates corresponding to the full map (a); dipole (b) quadrupole (c) and octopole (d). We have selected the direction of the preferred axis to coincide with the direction of the observed CMB dipole and used  $(r_0, \Omega_{X,in}) = (3.37 \text{ Gpc}, 0.69)$ ,  $r_{obs} = 30 \text{ Mpc}$  (from [86]).



#### 4. Conclusions

It has become evident during the last few years that early hints for deviation from the cosmological principle and statistical isotropy are being accumulated. This appears to be one of the most likely directions which may lead to new fundamental physics in the coming years. We have reviewed these hints, including the large scale CMB anomalies (CMB asymmetries), the large scale peculiar velocity flows on scales of 100 Mpc and up to a Gpc (dark flow), the preliminary evidence for the spatial variation of the fine structure constant along a preferred axis on Gpc scales, the coherent variation of quasar optical polarization on Gpc scales, the existence of the Large Quasar Structure with a Gpc scale and the mild hints for anisotropic expansion rate. We have pointed out the fact that most of the above cosmological observations are associated with the existence of specific cosmological directions which appear to be abnormally aligned with each other.

The Gpc scale associated with most of these effects indicates that their physical origin has appeared at late cosmological times. This possibility is further amplified by the fact that the CMB power asymmetry is significantly diminished if the ISW effect is subtracted from the CMB maps [94]. It is therefore natural to attempt to associate the physical origin of these effects with large scale dark energy or matter inhomogeneities. Hubble scale matter inhomogeneities in the form of voids are severely constrained by cosmological observations and are practically ruled out. On the other hand, dark energy Hubble scale inhomogeneities are observationally viable and reduce to standard  $\Lambda$ CDM when the inhomogeneity scale exceeds the horizon scale. A simple mechanism that can give rise to a cosmological preferred axis is based on an off-center observer in a spherical dark energy inhomogeneity. We have shown that this mechanism can naturally give rise to the observed alignment of many of the above described cosmic anisotropies.

The repulsive gravity properties of dark energy and its high sound velocity imply that any large scale dark energy inhomogeneity would tend to smooth out. This is a challenge for the above described mechanism. Nontrivial topology however can lead to sustainable Hubble scale dark energy inhomogeneities. If we happen to leave in the core of a Hubble scale recently formed topological defect we would naturally experience Hubble scale dark energy inhomogeneities and the existence of a preferred axis due to our displacement from the defect center. Therefore, topological quintessence constitutes a physical mechanism to produce Hubble scale dark energy inhomogeneities. We have shown that such a mechanism can also give rise to a Dark Energy Dipole, Large Scale Velocity Flows, Fine Structure Constant Dipole and a CMB Temperature Asymmetry aligned with each other. Other effects which may also occur (quasar polarization alignment etc) constitute interesting potential extensions of this research direction.

#### Acknowledgments

This research has been co-financed by the European Union (European Social Fund–ESF) and Greek national funds through the Operational Program “Education and Lifelong Learning” of the National Strategic Reference Framework (NSRF)–Research Funding Program: ARISTEIA. Investing in the society of knowledge through the European Social Fund.

## Conflicts of Interest

The author declares no conflict of interest.

## References

1. Hamilton, J.-C. What have we learned from observational cosmology? *ArXiv E-Prints*, **2013**, [arXiv:1304.4446](https://arxiv.org/abs/1304.4446).
2. Komatsu, E.; Smith, K.M.; Dunkley, J.; Bennett, C.L.; Gold, B.; Hinshaw, G.; Jarosik, N.; Larson, D.; Nolta, M.R.; Page, L.; *et al.* Seven-year Wilkinson Microwave Anisotropy Probe (WMAP) observations: Cosmological interpretation. *Astrophys. J.* **2011**, *192*, doi:10.1088/0067-0049/192/2/18.
3. Tegmark, M.; de Oliveira-Costa, A.; Hamilton, A. A high resolution foreground cleaned CMB map from WMAP. *Phys. Rev. D* **2003**, *68*, 123523, doi:10.1103/PhysRevD.68.123523.
4. Copi, C.J.; Huterer, D.; Schwarz, D.J.; Starkman, G.D. Large angle anomalies in the CMB. *Adv. Astron.* **2010**, *2010*, 847541, doi:10.1155/2010/847541.
5. Bennett, C.L.; Hill, R.S.; Hinshaw, G.; Larson, D.; Smith, K.M.; Dunkley, J.; Gold, B.; Halpern, M.; Jarosik, N.; Kogut, A.; *et al.* Seven-year Wilkinson Microwave Anisotropy Probe (WMAP) observations: Are there cosmic microwave background anomalies? *Astrophys. J.* **2011**, *192*, doi:10.1088/0067-0049/192/2/17.
6. Schwarz, D.J.; Starkman, G.D.; Huterer, D.; Copi, C.J. Is the low- $l$  microwave background cosmic? *Phys. Rev. Lett.* **2004**, *93*, 221301, doi:10.1103/PhysRevLett.93.221301.
7. Land, K.; Magueijo, J. The axis of evil. *Phys. Rev. Lett.* **2005**, *95*, 071301, doi:10.1103/PhysRevLett.95.071301.
8. Gruppuso, A.; Gorski, K.M. Large scale directional anomalies in the WMAP 5yr ILC map. *J. Cosmol. Astropart. Phys.* **2010**, *2010*, 019, doi:10.1088/1475-7516/2010/03/019.
9. Sarkar, D.; Huterer, D.; Copi, C.J.; Starkman, G.D.; Schwarz, D.J. Missing power vs. low- $l$  alignments in the cosmic microwave background: No correlation in the standard cosmological model. *ArXiv E-Prints*, **2010**, [arXiv:1004.3784](https://arxiv.org/abs/1004.3784).
10. Hanson, D.; Lewis, A. Estimators for CMB statistical anisotropy. *Phys. Rev. D.* **2009**, *80*, 063004, doi:10.1103/PhysRevD.80.063004.
11. Copi, C.J.; Huterer, D.; Schwarz, D.J.; Starkman, G.D. The uncorrelated universe: Statistical anisotropy and the vanishing angular correlation function in WMAP years 1–3. *Phys. Rev. D* **2007**, *75*, 023507, doi:10.1103/PhysRevD.75.023507.
12. Smith, K.M.; Senatore, L.; Zaldarriaga, M. Optimal limits on  $f_{NL}^{local}$  from WMAP 5-year data. *J. Cosmol. Astropart. Phys.* **2009**, *2009*, 006, doi:10.1088/1475-7516/2009/09/006.
13. Ade, P.A.R.; Aghanim, N.; Armitage-Caplan, C.; Arnaud, M.; Ashdown, M.; Atrio-Barandela, F.; Aumont, J.; Baccigalupi, C.; Banday, A.J.; Barreiro, R.B.; *et al.* Planck 2013 results. I. Overview of products and scientific results. *ArXiv E-Prints*, **2013**, [arXiv:1303.5062](https://arxiv.org/abs/1303.5062).

14. Amanullah, R.; Lidman, C.; Rubin, D.; Aldering, G.; Astier, P.; Barbary, K.; Burns, M.S.; Conley, A.; Dawson, K.S.; Deustua, S.E.; *et al.* Spectra and light curves of six type Ia supernovae at  $0.511 < z < 1.12$  and the Union2 compilation. *Astrophys. J.* **2010**, *716*, 712, doi:10.1088/0004-637X/716/1/712.
15. Percival, W.J.; Cole, S.; Eisenstein, D.J.; Nichol, R.C.; Peacock, J.A.; Pope, A.C.; Szalay, A.S. Measuring the Baryon Acoustic Oscillation scale using the SDSS and 2dFGRS. *Mon. Not. R. Astron. Soc.* **2007**, *381*, 1053–1066.
16. Bueno Sanchez, J.C.; Nesseris, S.; Perivolaropoulos, L. Comparison of recent SnIa datasets. *J. Cosmol. Astropart. Phys.* **2009**, *2009*, 029, doi:10.1088/1475-7516/2009/11/029.
17. Nesseris, S.; Perivolaropoulos, L. Testing  $\Lambda$ CDM with the growth function  $\delta(a)$ : Current constraints. *Phys. Rev. D* **2008**, *77*, 023504, doi:10.1103/PhysRevD.77.023504.
18. Trujillo-Gomez, S.; Klypin, A.; Primack, J.; Romanowsky, A.J. LCDM correctly predicts basic statistics of galaxies: Luminosity-velocity relation, baryonic mass-velocity relation, and velocity function. *ArXiv E-Prints*, **2011**, arXiv:1005.1289.
19. Reid, B.A.; Percival, W.J.; Eisenstein, D.J.; Verde, L.; Spergel, D.N.; Skibba, R.A.; Bahcall, N.A.; Budavari, T.; Fukugita, M.; Richard Gott, J.; *et al.* Cosmological constraints from the clustering of the sloan digital sky survey DR7 luminous red galaxies. *Mon. Not. R. Astron. Soc.* **2010**, *404*, 60–85.
20. Perivolaropoulos, L. Six puzzles for LCDM cosmology. *ArXiv E-Prints*, **2008**, arXiv:0811.4684.
21. Yang, R.-J.; Zhang, S.N. The age problem in  $\Lambda$ CDM model. *Mon. Not. R. Astron. Soc.* **2010**, *407*, 1835–1841.
22. Ade, P.A.R.; Aghanim, N.; Armitage-Caplan, C.; Arnaud, M.; Ashdown, M.; Atrio-Barandela, F.; Aumont, J.; Baccigalupi, C.; Banday, A.J.; Barreiro, R.B.; *et al.* Planck 2013 results. XXIII. Isotropy and Statistics of the CMB. *ArXiv E-Prints*, **2013**, arXiv:1303.5083.
23. Eriksen, H.K.; Banday, A.J.; Gorski, K.M.; Hansen, F.K.; Lilje, P.B. Hemispherical power asymmetry in the third-year Wilkinson Microwave Anisotropy Probe sky maps. *Astrophys. J.* **2007**, *660*, L81, doi:10.1086/518091.
24. Paci, F.; Gruppuso, A.; Finelli, F.; Cabella, P.; de Rosa, A.; Mandolesi, N.; Natoli, P. Power asymmetries in the cosmic microwave background temperature and polarization patterns. *Mon. Not. R. Astron. Soc.* **2010**, *407*, 399–404.
25. Hoftuft, J.; Eriksen, H.K.; Banday, A.J.; Gorski, K.M.; Hansen, F.K.; Lilje, P.B. Increasing evidence for hemispherical power asymmetry in the five-year WMAP data. *Astrophys. J.* **2009**, *699*, 985, doi:10.1088/0004-637X/699/2/985.
26. Axelsson, M.; Fantaye, Y.; Hansen, F.K.; Banday, A.J.; Eriksen, H.K.; Gorski, K.M. Directional dependence of  $\Lambda$ CDM cosmological parameters. *Astrophys. J.* **2013**, *773*, L3, doi:10.1088/2041-8205/773/1/L3.
27. Mariano, A.; Perivolaropoulos, L. CMB maximum temperature asymmetry axis: Alignment with other cosmic asymmetries. *Phys. Rev. D* **2013**, *87*, 043511, doi:10.1103/PhysRevD.87.043511.
28. Watkins, R.; Feldman, H.A.; Hudson, M.J. Consistently large cosmic flows on scales of 100 Mpc/h: A challenge for the standard LCDM cosmology. *Mon. Not. R. Astron. Soc.* **2009**, *392*, 743–756.



29. Feldman, H.A.; Watkins, R.; Hudson, M.J. Cosmic flows on 100 Mpc/h scales: Standardized minimum variance bulk flow, shear and octupole moments. *Mon. Not. R. Astron. Soc.* **2010**, *407*, 2328–2338.
30. Kashlinsky, A.; Atrio-Barandela, F.; Kocevski, D.; Ebeling, H. A measurement of large-scale peculiar velocities of clusters of galaxies: Results and cosmological implications. *Astrophys. J.* **2008**, *686*, L49, doi:10.1086/592947.
31. Lavaux, G.; Tully, R.B.; Mohayaee, R.; Colombi, S. Cosmic flow from 2MASS redshift survey: The origin of CMB dipole and implications for LCDM cosmology. *Astrophys. J.* **2010**, *709*, 483, doi:10.1088/0004-637X/709/1/483.
32. Hutsemekers, D.; Lamy, H. The polarization properties of broad absorption line QSOs: Observational results. *ArXiv E-Prints*, **2001**, arXiv:astro-ph/0109528.
33. Hutsemekers, D.; Cabanac, R.; Lamy, H.; Sluse, D. Mapping extreme-scale alignments of quasar polarization vectors. *Astron. Astrophys.* **2005**, *441*, 915, doi:10.1051/0004-6361:20053337.
34. Hutsemekers, D.; Payez, A.; Cabanac, R.; Lamy, H.; Sluse, D.; Borguet, B.; Cudell, J.R. Large-scale alignments of quasar polarization vectors: Evidence at cosmological scales for very light pseudoscalar particles mixing with photons? *ArXiv E-Prints*, **2008**, arXiv:0809.3088.
35. Mariano, A.; Perivolaropoulos, L. Is there correlation between fine structure and dark energy cosmic dipoles? *Phys. Rev. D* **2012**, *86*, 083517, doi:10.1103/PhysRevD.86.083517.
36. Webb, J.K.; King, J.A.; Murphy, M.T.; Flambaum, V.V.; Carswell, R.F.; Bainbridge, M.B. Indications of a spatial variation of the fine structure constant. *Phys. Rev. Lett.* **2011**, *107*, 191101, doi:10.1103/PhysRevLett.107.191101.
37. King, J.A.; Webb, J.K.; Murphy, M.T.; Flambaum, V.V.; Carswell, R.F.; Bainbridge, M.B.; Wilczynska, M.R.; Koch, F.E. Spatial variation in the fine-structure constant—New results from VLT/UVES. *Mon. Not. R. Astron. Soc.* **2012**, *422*, 3370–3414.
38. Clowes, R.G.; Harris, K.A.; Raghunathan, S.; Campusano, L.E.; Soechting, I.K.; Graham, M.J. A structure in the early universe at  $z \sim 1.3$  that exceeds the homogeneity scale of the R-W concordance cosmology. *ArXiv E-Prints*, **2012**, arXiv:1211.6256.
39. Gott, J.R., III; Juric, M.; Schlegel, D.; Hoyle, F.; Vogeley, M.; Tegmark, M.; Bahcall, N.; Brinkmann, J. A map of the universe. *Astrophys. J.* **2005**, *624*, 463, doi:10.1086/428890.
40. Yadav, J.K.; Bagla, J.S.; Khandai, N. Fractal dimension as a measure of the scale of homogeneity. *Mon. Not. R. Astron. Soc.* **2010**, *405*, 2009–2015.
41. Luminet, J.-P. The shape and topology of the universe. *ArXiv E-Prints*, **2008**, arXiv:0802.2236.
42. Bielewicz, P.; Riazuelo, A. The study of topology of the universe using multipole vectors. *ArXiv E-Prints*, **2009**, arXiv:0804.2437.
43. Carneiro, S.; Mena Marugan, G.A. Anisotropic cosmologies containing isotropic background radiation. *Phys. Rev. D* **2001**, *64*, 083502, doi:10.1103/PhysRevD.64.083502.
44. Akofer, E.; Balachandran, A.P.; Jo, S.G.; Joseph, A.; Qureshi, B.A. Direction-dependent CMB power spectrum and statistical anisotropy from noncommutative geometry. *J. High Energy Phys.* **2008**, *2008*, 092, doi:10.1088/1126-6708/2008/05/092.
45. Koivisto, T.S.; Mota, D.F.; Quartin, M.; Zlosnik, T.G. On the possibility of anisotropic curvature in cosmology. *Phys. Rev. D* **2011**, *83*, 023509, doi:10.1103/PhysRevD.83.023509.

46. Zumalacarregui, M.; Koivisto, T.S.; Mota, D.F.; Ruiz-Lapuente, P. Disformalscalar fields and the dark sector of the universe. *J. Cosmol. Astropart. Phys.* **2010**, *2010*, 038, doi:10.1088/1475-7516/2010/05/038.
47. Koivisto, T.; Mota, D.F. Dark energy anisotropic stress and large scale structure formation. *Phys. Rev. D* **2006**, *73*, 083502, doi:10.1103/PhysRevD.73.083502.
48. Battye, R.; Moss, A. Anisotropic dark energy and CMB anomalies. *Phys. Rev. D* **2009**, *80*, 023531, doi:10.1103/PhysRevD.80.023531.
49. Armendariz-Picon, C. Could dark energy be vector-like? *J. Cosmol. Astropart. Phys.* **2004**, *2004*, 007, doi:10.1088/1475-7516/2004/07/007.
50. Esposito-Farese, G.; Pitrou, C.; Uzan, J.-P. Vector theories in cosmology. *Phys. Rev. D* **2010**, *81*, 063519, doi:10.1103/PhysRevD.81.063519.
51. Rodrigues, D.C. Anisotropic cosmological constant and the CMB quadrupole anomaly. *Phys. Rev. D* **2008**, *77*, 023534, doi:10.1103/PhysRevD.77.023534.
52. Jimenez, J.B.; Maroto, A.L. Large-scale cosmic flows and moving dark energy model for anisotropization. *J. Cosmol. Astropart. Phys.* **2009**, *2009*, 015, doi:10.1088/1475-7516/2009/03/015.
53. Alexander, S.; Biswas, T.; Notari, A.; Vaid, D. Local void vs. dark energy: Confrontation with wmap and type Ia supernovae. *J. Cosmol. Astropart. Phys.* **2009**, *2009*, 025, doi:10.1088/1475-7516/2009/09/025.
54. Garcia-Bellido, J.; Haugboelle, T. Confronting Lemaître-Tolman-Bondi models with observational cosmology. *J. Cosmol. Astropart. Phys.* **2008**, *2008*, 003, doi:10.1088/1475-7516/2008/04/003.
55. Biswas, T.; Notari, A.; Valkenburg, W. Testing the void against cosmological data: Fitting CMB, BAO, SN and  $H_0$ . *J. Cosmol. Astropart. Phys.* **2010**, *2010*, 030, doi:10.1088/1475-7516/2010/11/030.
56. Dunsby, P.; Goheer, N.; Osano, B.; Uzan, J.P. How close can an inhomogeneous universe mimic the concordance model? *J. Cosmol. Astropart. Phys.* **2010**, *2010*, 017, doi:10.1088/1475-7516/2010/06/017.
57. Garfinkle, D. The motion of galaxy clusters in inhomogeneous cosmologies. *Class. Quantum Gravity* **2010**, *27*, 065002, doi:10.1088/0264-9381/27/6/065002.
58. Krasinski, A. *Inhomogeneous Cosmological Models*; Cambridge University Press: Cambridge, UK, 1997.
59. Bolejko, K.; Celerier, M.-N.; Krasinski, A. Inhomogeneous cosmological models: Exact solutions and their applications. *Class. Quantum Gravity* **2011**, *28*, 164002, doi:10.1088/0264-9381/28/16/164002.
60. Alnes, H.; Amarzguioui, M.; Gron, O. An inhomogeneous alternative to dark energy? *Phys. Rev. D* **2006**, *73*, 083519, doi:10.1103/PhysRevD.73.083519.
61. Armendariz-Picon, C. Creating statistically anisotropic and inhomogeneous perturbations. *J. Cosmol. Astropart. Phys.* **2007**, *2007*, 014, doi:10.1088/1475-7516/2007/09/014.

62. Pullen, A.R.; Kamionkowski, M. Cosmic microwave background statistics for a direction-dependent primordial power spectrum. *Phys. Rev. D* **2007**, *76*, 103529, doi:10.1103/PhysRevD.76.103529.
63. Ackerman, L.; Carroll, S.M.; Wise, M.B. Imprints of a primordial preferred direction on the microwave background. *Phys. Rev. D* **2007**, *75*, 083502, doi:10.1103/PhysRevD.75.083502.
64. Valenzuela-Toledo, C.A. Non-gaussianity and statistical anisotropy in cosmological inflationary models. *ArXiv E-Prints*, **2010**, arXiv:1004.5363.
65. Dimopoulos, K.; Karciuskas, M.; Lyth, D.H.; Rodriguez, Y. Statistical anisotropy of the curvature perturbation from vector field perturbations. *J. Cosmol. Astropart. Phys.* **2009**, *2009*, 013, doi:10.1088/1475-7516/2009/05/013.
66. Yokoyama, S.; Soda, J. Primordial statistical anisotropy generated at the end of inflation. *J. Cosmol. Astropart. Phys.* **2008**, *2008*, 005, doi:10.1088/1475-7516/2008/08/005.
67. Golovnev, A.; Vanchurin, V. Cosmological perturbations from vector inflation. *Phys. Rev. D* **2009**, *79*, 103524, doi:10.1103/PhysRevD.79.103524.
68. Bartolo, N.; Dimastrogiovanni, E.; Matarrese, S.; Riotto, A. Anisotropic bispectrum of curvature perturbations from primordial non-Abelian vector fields. *J. Cosmol. Astropart. Phys.* **2009**, *2009*, 015, doi:10.1088/1475-7516/2009/10/015.
69. Himmetoglu, B.; Contaldi, C.R.; Peloso, M. Instability of anisotropic cosmological solutions supported by vector fields. *Phys. Rev. Lett.* **2009**, *102*, 111301, doi:10.1103/PhysRevLett.102.111301.
70. Himmetoglu, B.; Contaldi, C.R.; Peloso, M. Instability of the ACW model, and problems with massive vectors during inflation. *Phys. Rev. D* **2009**, *79*, 063517, doi:10.1103/PhysRevD.79.063517.
71. Himmetoglu, B.; Contaldi, C.R.; Peloso, M. Ghost instabilities of cosmological models with vector fields nonminimally coupled to the curvature. *Phys. Rev. D* **2009**, *80*, 123530, doi:10.1103/PhysRevD.80.123530.
72. Thorsrud, M.; Mota, D.F.; Hervik, S. Cosmology of a scalar field coupled to matter and an isotropy-violating Maxwell field. *J. High Energy Phys.* **2012**, *2012*, 066, doi:10.1007/JHEP10(2012)066.
73. Kahniashvili, T.; Lavrelashvili, G.; Ratra, B. CMB temperature anisotropy from broken spatial isotropy due to an homogeneous cosmological magnetic field. *Phys. Rev. D* **2008**, *78*, 063012, doi:10.1103/PhysRevD.78.063012.
74. Barrow, J.D.; Ferreira, P.G.; Silk, J. Constraints on a primordial magnetic field. *Phys. Rev. Lett.* **1997**, *78*, 3610–3613.
75. Campanelli, L. A model of universe anisotropization. *Phys. Rev. D* **2009**, *80*, 063006, doi:10.1103/PhysRevD.80.063006.
76. Kim, J.; Naselsky, P. Cosmological Alfvén waves in the recent CMB data, and the observational bound on the primordial vector perturbation. *J. Cosmol. Astropart. Phys.* **2009**, *2009*, 041, doi:10.1088/1475-7516/2009/07/041.

77. Bueno Sanchez, J.C.; Perivolaropoulos, L. Dark energy and matter perturbations in scalar-tensor theories of gravity. *J. Phys. Conf. Ser.* **2011**, *283*, 012006, doi:10.1088/1742-6596/283/1/012006.
78. Bean, R.; Dore, O. Probing dark energy perturbations: The dark energy equation of state and speed of sound as measured by WMAP. *Phys. Rev. D* **2004**, *69*, 083503, doi:10.1103/PhysRevD.69.083503.
79. Bueno Sanchez, J.C.; Perivolaropoulos, L. Topological quintessence. *Phys. Rev. D* **2011**, *84*, 123516, doi:10.1103/PhysRevD.84.123516.
80. Marra, V.; Notari, A. Observational constraints on inhomogeneous cosmological models without dark energy. *Class. Quantum Gravity* **2011**, *28*, 164004, doi:10.1088/0264-9381/28/16/164004.
81. Zumalacarregui, M.; Garcia-Bellido, J.; Ruiz-Lapuente, P. Tension in the void: Cosmic rulers strain inhomogeneous cosmologies. *J. Cosmol. Astropart. Phys.* **2012**, *2012*, 009, doi:10.1088/1475-7516/2012/10/009.
82. Caldwell, R.R.; Stebbins, A. A test of the copernican principle. *Phys. Rev. Lett.* **2008**, *100*, 191302, doi:10.1103/PhysRevLett.100.191302.
83. Garcia-Bellido, J.; Haugboelle, T. Looking the void in the eyes—The kinematic Sunyaev–Zeldovich effect in Lemaître–Tolman–Bondi models. *J. Cosmol. Astropart. Phys.* **2008**, *2008*, 016, doi:10.1088/1475-7516/2008/09/016.
84. Ricciardelli, E.; Quilis, V.; Planelles, S. The structure of cosmic voids in a LCDM Universe. *ArXiv E-Prints*, **2013**, [arXiv:1306.2955](https://arxiv.org/abs/1306.2955).
85. Alnes, H.; Amarzguioui, M. CMB anisotropies seen by an off-center observer in a spherically symmetric inhomogeneous Universe. *Phys. Rev. D* **2006**, *74*, 103520, doi:10.1103/PhysRevD.74.103520.
86. Grande, J.; Perivolaropoulos, L. Generalized Lemaître–Tolman–Bondi model with inhomogeneous isotropic dark energy: Observational constraints. *Phys. Rev. D* **2011**, *84*, 023514, doi:10.1103/PhysRevD.84.023514.
87. Vilenkin, A. Topological inflation. *Phys. Rev. Lett.* **1994**, *72*, 3137–3140.
88. Hansen, F.K.; Banday, A.J.; Gorski, K.M.; Eriksen, H.K.; Lilje, P.B. Power asymmetry in cosmic microwave background fluctuations from full sky to sub-degree scales: Is the universe isotropic? *Astrophys. J.* **2009**, *704*, 1448, doi:10.1088/0004-637X/704/2/1448.
89. Eriksen, H.K.; Hansen, F.K.; Banday, A.J.; Gorski, K.M.; Lilje, P.B. Asymmetries in the cosmic microwave background anisotropy field. *Astrophys. J.* **2004**, *605*, 14, doi:10.1086/382267.
90. Park, C.-G. Non-Gaussian signatures in the temperature fluctuation observed by the Wilkinson Microwave Anisotropy Probe. *Mon. Not. R. Astron. Soc.* **2004**, *349*, 313–320.
91. Hirata, C.M. Constraints on cosmic hemispherical power anomalies from quasars. *J. Cosmol. Astropart. Phys.* **2009**, *2009*, 011, doi:10.1088/1475-7516/2009/09/011.
92. Dai, L.; Jeong, D.; Kamionkowski, M.; Chluba, J. The pesky power asymmetry. *Phys. Rev. D* **2013**, *87*, 123005, doi:10.1103/PhysRevD.87.123005.
93. Chang, Z.; Wang, S. Inflation and primordial power spectra at anisotropic spacetime inspired by Planck’s constraints on isotropy of CMB. *Eur. Phys. J. C* **2013**, *73*, 2516, doi:10.1140/epjc/s10052-013-2516-5.

94. Rassat, A.; Starck, J.-L. On Preferred Axes in WMAP cosmic microwave background data after subtraction of the integrated Sachs-Wolfe effect. *ArXiv E-Prints*, **2013**, [arXiv:1303.5051](https://arxiv.org/abs/1303.5051).
95. Bielewicz, P.; Gorski, K.M.; Banday, A.J. Low-order multipole maps of CMB anisotropy derived from WMAP. *Mon. Not. R. Astron. Soc.* **2004**, *355*, 1283–1302.
96. Frommert, M.; Ensslin, T.A. The axis of evil—A polarization perspective. *Mon. Not. R. Astron. Soc.* **2010**, *403*, 1739–1748.
97. Land, K.; Magueijo, J. Is the Universe odd? *Phys. Rev. D* **2005**, *72*, 101302, doi:10.1103/PhysRevD.72.101302.
98. Land, K.; Magueijo, J. Cubic anomalies in WMAP. *Mon. Not. R. Astron. Soc.* **2005**, *357*, 994, doi:10.1111/j.1365-2966.2005.08707.x/abs/.
99. Park, C.-G.; Park, C.; Gott, J.R., III. Cleaned 3 year Wilkinson Microwave Anisotropy Probe Cosmic Microwave Background map: Magnitude of the quadrupole and alignment of large-scale modes. *Astrophys. J.* **2007**, *660*, 959, doi:10.1086/513455.
100. De Oliveira-Costa, A.; Tegmark, M. CMB multipole measurements in the presence of foregrounds. *Phys. Rev. D* **2006**, *74*, 023005, doi:10.1103/PhysRevD.74.023005.
101. Naselsky, P.D.; Verkhodanov, O.V.; Chiang, L.-Y.; Novikov, I.D. Phase analysis of the 1-year WMAP data and its application for the CMB foreground separation. *ArXiv E-Prints*, **2003**, [arXiv:astro-ph/0310235](https://arxiv.org/abs/astro-ph/0310235).
102. Lineweaver, C.H.; Tenorio, L.; Smoot, G.F.; Keegstra, P.; Banday, A.J.; Lubin, P. The dipole observed in the COBE DMR 4 year data. *Astrophys. J.* **1996**, *470*, 38, doi: 10.1086/177846.
103. Kashlinsky, A.; Atrio-Barandela, F. Measuring cosmological bulk flows via the kinematic Sunyaev-Zeldovich effect in the upcoming cosmic microwave background maps. *Astrophys. J.* **2000**, *536*, L67, doi:10.1086/312735.
104. Kashlinsky, A.; Atrio-Barandela, F.; Ebeling, H.; Edge, A.; Kocevski, D. A new measurement of the bulk flow of X-ray luminous clusters of galaxies. *Astrophys. J.* **2010**, *712*, L81, doi:10.1088/2041-8205/712/1/L81.
105. Atrio-Barandela, F.; Kashlinsky, A.; Ebeling, H.; Kocevski, D. Cosmic Microwave Background filters and the Dark-Flow measurement. *ArXiv E-Prints*, **2013**, [arXiv:1211.4345](https://arxiv.org/abs/1211.4345).
106. Ade, P.A.R.; Aghanim, N.; Arnaud, M.; Ashdown, M.; Aumont, J.; Baccigalupi, C.; Balbi, A.; Banday, A.J.; Barreiro, R.B.; Battaner, E.; *et al.* Planck intermediate results. XIII. Constraints on peculiar velocities. *ArXiv E-Prints*, **2013**, [arXiv:1303.5090](https://arxiv.org/abs/1303.5090).
107. Hand, N.; Addison, G.E.; Aubourg, E.; Battaglia, N.; Battistelli, E.S.; Bizyaev, D.; Bond, J.R.; Brewington, H.; Brinkmann, J.; Brown, B.R.; *et al.* Evidence of galaxy cluster motions with the kinematic Sunyaev-Zel’dovich effect. *Phys. Rev. Lett.* **2012**, *109*, 041101, doi:10.1103/PhysRevLett.109.041101.
108. Keisler, R. The statistical significance of the “dark flow”. *Astrophys. J.* **2009**, *707*, L42, doi:10.1088/0004-637X/707/1/L42.
109. Osborne, S.J.; Mak, D.S.Y.; Church, S.E.; Pierpaoli, E. Measuring the galaxy cluster bulk flow from WMAP data. *Astrophys. J.* **2011**, *737*, 98, doi:10.1088/0004-637X/737/2/98.

110. Mody, K.; Hajian, A. One thousand and one clusters: Measuring the bulk flow with the planck ESZ and X-ray selected galaxy cluster catalogs. *Astrophys. J.* **2012**, *758*, 4, doi:10.1088/0004-637X/758/1/4.
111. Atrio-Barandela, F. On the statistical significance of the bulk flow measured by the PLANCK satellite. *ArXiv E-Prints*, **2013**, [arXiv:1303.6614](https://arxiv.org/abs/1303.6614).
112. Turnbull, S.J.; Hudson, M.J.; Feldman, H.A.; Hicken, M.; Kirshner, R.P.; Watkins, R. Cosmic flows in the nearby universe from Type Ia supernovae. *Mon. Not. R. Astron. Soc.* **2012**, *420*, 447–454.
113. Dai, D.-C.; Kinney, W.H.; Stojkovic, D. Measuring the cosmological bulk flow using the peculiar velocities of supernovae. *J. Cosmol. Astropart. Phys.* **2011**, *2011*, 015, doi:10.1088/1475-7516/2011/04/015.
114. Payez, A.; Cudell, J.R.; Hutsemekers, D. Axions and polarisation of quasars. *AIP Conf. Proc.* **2008**, *1038*, 211, doi:10.1063/1.2987174.
115. Tiwari, P.; Jain, P. Polarization Alignment in JVAS/CLASS flat spectrum radio surveys. *Int. J. Mod. Phys. D* **2013**, *22*, 1350089, doi:10.1142/S0218271813500892.
116. Payez, A. Cornering the axionlike particle explanation of quasar polarisations. *Phys. Rev. D* **2012**, *85*, 087701, doi:10.1103/PhysRevD.85.087701.
117. Payez, A.; Cudell, J.R.; Hutsemekers, D. Can axionlike particles explain the alignments of the polarisations of light from quasars? *Phys. Rev. D* **2011**, *84*, 085029, doi:10.1103/PhysRevD.84.085029.
118. Kalus, B.; Schwarz, D.J.; Seikel, M.; Wiegand, A. Constraints on anisotropic cosmic expansion from supernovae. *Astron. Astrophys.* **2013**, *553*, A56, doi:10.1051/0004-6361/201220928.
119. Colin, J.; Mohayaee, R.; Sarkar, S.; Shafieloo, A. Probing the anisotropic local universe and beyond with SNe Ia data. *Mon. Not. R. Astron. Soc.* **2011**, *414*, 264–271.
120. Schwarz, D.J.; Weinhorst, B. (An)isotropy of the Hubble diagram: Comparing hemispheres. *Astron. Astrophys.* **2007**, *474*, 717–729.
121. Cai, R.-G.; Tuo, Z.-L. Direction dependence of the deceleration parameter. *J. Cosmol. Astropart. Phys.* **2012**, *2012*, 004, doi:10.1088/1475-7516/2012/02/004.
122. Campanelli, L.; Cea, P.; Fogli, G.L.; Marrone, A. Testing the isotropy of the Universe with type Ia supernovae. *Phys. Rev. D* **2011**, *83*, 103503, doi:10.1103/PhysRevD.83.103503.
123. Antoniou, I.; Perivolaropoulos, L. Searching for a cosmological preferred axis: Union2 data analysis and comparison with other probes. *J. Cosmol. Astropart. Phys.* **2010**, *2010*, 012, doi:10.1088/1475-7516/2010/12/012.
124. Zhao, W.; Wu, P.X.; Zhang, Y. Anisotropy of cosmic acceleration. *Int. J. Mod. Phys. D* **2013**, *22*, 1350060, doi: 10.1142/S0218271813500600.
125. Cai, R.-G.; Ma, Y.-Z.; Tang, B.; Tuo, Z.-L. Constraining the anisotropic expansion of the Universe. *Phys. Rev. D* **2013**, *87*, 123522, doi:10.1103/PhysRevD.87.123522.
126. Blomqvist, M.; Mortsell, E.; Nobili, S. Probing dark energy inhomogeneities with supernovae. *J. Cosmol. Astropart. Phys.* **2008**, *2008*, 027, doi:10.1088/1475-7516/2008/06/027.
127. Blomqvist, M.; Enander, J.; Mortsell, E. Constraining dark energy fluctuations with supernova correlations. *J. Cosmol. Astropart. Phys.* **2010**, *2010*, 018, doi:10.1088/1475-7516/2010/10/018.

128. Cooke, R.; Lynden-Bell, D. Does the Universe accelerate equally in all directions? *Mon. Not. R. Astron. Soc.* **2010**, *401*, 1409–1414.
129. Gupta, S.; Saini, T.D. Direction dependence in supernova data: Constraining isotropy. *Mon. Not. R. Astron. Soc.* **2010**, *407*, 651–657.
130. Cameron, E.; Pettitt, T. On the evidence for cosmic variation of the fine structure constant (I): A Parametric Bayesian model selection analysis of the quasar dataset. *ArXiv E-Prints*, **2013**, [arXiv:1207.6223](https://arxiv.org/abs/1207.6223).
131. Kanekar, N.; Langston, G.I.; Stocke, J.T.; Carilli, C.L.; Menten, K.L. Constraining fundamental constant evolution with HI and OH lines. *Astrophys. J.* **2012**, *746*, L16, doi:10.1088/2041-8205/746/2/L16.
132. Levshakov, S.A.; Combes, F.; Boone, F.; Agafonova, I.I.; Reimers, D.; Kozlov, M.G. An upper limit to the variation in the fundamental constants at redshift  $z = 5.2$ . *Astron. Astrophys.* **2012**, *540*, L9, doi:10.1051/0004-6361/201219042.
133. Marinoni, C.; Bel, J.; Buzzi, A. The scale of cosmic isotropy. *J. Cosmol. Astropart. Phys.* **2012**, *2012*, 036, doi:10.1088/1475-7516/2012/10/036.
134. Schneider, D.P.; Richards, G.T.; Hall, P.B.; Strauss, M.A.; Anderson, S.F.; Boroson, T.A.; Ross, N.P.; Shen, Y.; Brandt, W.N.; Fan, X.; *et al.* The sloan digital sky survey quasar catalog. V. seventh data release. *Astron. J.* **2010**, *139*, 2360, doi:10.1088/0004-6256/139/6/2360.
135. Nadathur, S. Seeing patterns in noise: Gigaparsec-scale “structures” that do not violate homogeneity. *Mon. Not. R. Astron. Soc.* **2013**, *434*, 398–406.
136. Pilipenko, S.; Malinovsky, A. Testing statistical significance of large quasar groups with sheets model of large scale structure. *ArXiv E-Prints*, **2013**, [arXiv:1306.3970](https://arxiv.org/abs/1306.3970).
137. Koivisto, T.; Mota, D.F. Accelerating cosmologies with an anisotropic equation of state. *Astrophys. J.* **2008**, *679*, 1, doi:10.1086/587451.
138. Mota, D.F.; Kristiansen, J.R.; Koivisto, T.; Groeneboom, N.E. Constraining dark energy anisotropic stress. *Mon. Not. R. Astron. Soc.* **2007**, *382*, 793–800.
139. Koivisto, T.; Mota, D.F. Anisotropic dark energy: Dynamics of background and perturbations. *J. Cosmol. Astropart. Phys.* **2008**, *2008*, 018, doi:10.1088/1475-7516/2008/06/018.
140. Lemaître, A.G. The expanding universe. *Gen. Relativ. Gravit.* **1997**, *29*, 641–680.
141. Tolman, R.C. Effect of inhomogeneity on cosmological models. *Proc. Natl. Acad. Sci. USA* **1934**, *20*, 169–176.
142. Bondi, H. Spherically symmetrical models in general relativity. *Mon. Not. R. Astron. Soc.* **1947**, *107*, 410–425.
143. Enqvist, K.; Mattsson, T. The effect of inhomogeneous expansion on the supernova observations. *J. Cosmol. Astropart. Phys.* **2007**, *2007*, 019, doi:10.1088/1475-7516/2007/02/019.
144. Alnes, H.; Amarzguioui, M. The supernova Hubble diagram for off-center observers in a spherically symmetric inhomogeneous Universe. *Phys. Rev. D* **2007**, *75*, 023506, doi:10.1103/PhysRevD.75.023506.
145. Szekeres, P. Quasispherical Gravitational Collapse. *Phys. Rev. D* **1975**, *12*, 2941–2948.
146. Szekeres, P. A class of inhomogeneous cosmological models. *Commun. Math. Phys.* **1975**, *41*, 55–64.

147. Goode, S.W.; Wainwright, J. Singularities and evolution of the Szekeres cosmological models. *Phys. Rev. D* **1982**, *26*, 3315–3326.
148. Bonnor, W.B. Non-radiative solutions of Einstein's equations for dust. *Commun. Math. Phys.* **1976**, *51*, 191–199.
149. Cho, I.; Vilenkin, A. Spacetime structure of an inflating global monopole. *Phys. Rev. D* **1997**, *56*, 7621–7626.
150. Bekenstein, J.D. Fine-structure constant: Is it really a constant? *Phys. Rev. D* **1982**, *25*, 1527–1539.
151. Sandvik, H.B.; Barrow, J.D.; Magueijo, J. A simple cosmology with a varying fine structure constant. *Phys. Rev. Lett.* **2002**, *88*, 031302, doi:10.1103/PhysRevLett.88.031302.
152. Avgoustidis, A.; Martins, C.J.A.P.; Monteiro, A.M.R.V.L.; Vielzeuf, P.E.; Luzzi, G. Cosmological effects of scalar-photon couplings: Dark energy and varying- $\alpha$  models. *ArXiv E-Prints*, **2013**, [arXiv:1305.7031](https://arxiv.org/abs/1305.7031).
153. Sakai, N.; Shinkai, H.-A.; Tachizawa, T.; Maeda, K.-I. Dynamics of topological defects and inflation. *Phys. Rev. D* **1996**, *53*, 655–661.
154. Barriola, M.; Vilenkin, A. Gravitational field of a global monopole. *Phys. Rev. Lett.* **1989**, *63*, 341–343.
155. Balcerzak, A.; Dabrowski, M.P.; Denkiewicz, T. Off-center observers versus supernovae in inhomogeneous pressure universes. *ArXiv E-Prints*, **2013**, [arXiv:1312.1567](https://arxiv.org/abs/1312.1567).
156. Lineweaver, C.H. The CMB dipole: The most recent measurement and some history. *ArXiv E-Prints*, **1996**, [arXiv:astro-ph/9609034](https://arxiv.org/abs/astro-ph/9609034).

© 2014 by the author; licensee MDPI, Basel, Switzerland. This article is an open access article distributed under the terms and conditions of the Creative Commons Attribution license (<http://creativecommons.org/licenses/by/3.0/>).